MODELING AND SIMULATION OF FLOW PATTERN AND CURING DURING MANUFACTURING OF COMPOSITE WIND TURBINE BLADES USING VARTM PROCESS

A Thesis by

Ramin Karaminezhaad Ranjbar

Bachelor of Science, University of Kerman, 2003

Submitted to the Department of Mechanical Engineering
and the faculty of the Graduate School of
Wichita State University
in Partial fulfillment of
the requirements for the degree of
Master of Science

May 2010

MODELING AND SIMULATION OF FLOW PATTERN AND CURING DURING MANUFACTURING OF COMPOSITE WIND TURBINE BLADES USING VARTM PROCESS

The following faculty members have examined the final copy of this thesis for form and content, and recommend that it be accepted in partial fulfillment of the requirement for the degree of Master of Science with a major in Mechanical Engineering.

_____
Bob Minaie, Committee Chair

_____
Krishna Krishnan, Committee Member

_____
Hamid Lankarani, Committee Member

DEDICATION

To my daughter, Kimia, who always made the headaches go away.

ACKNOWLEDGEMENTS

I would like to thank my advisor, Professor Bob Minaie, for his support and useful suggestions. I am grateful to Professor Krishna Krishnan and Professor Hamid Lankarani for serving on my thesis committee.

Special thanks go to Alejandro Rodriguez for his valuable comments throughout this work. I thank my colleagues Seyed Soltani, Mostafa Sabzevari, Behrouz Tavakol, Chee Sern Lim, Hoda Koushyar and Mauricio Guzman in Professor Minaie's research group for their friendship. I would also like to thank my family who are always supportive and caring.

Financial support by the Department of Energy is gratefully acknowledged.

ABSTRACT

Vacuum-Assisted Resin Transfer Molding (VARTM) has become a widly used and rapidly growing manufacturing process for wind turbine blades. However, in the case of complex geometries, resin flow pattern during the VARTM process tends to be unpredictable. In addition, increasing the size and thickness of the blades is expected to result in additional technical difficulties. Therefore, use of flow pattern simulation tools has become a necessity in order to avoid costly and time-consuming trial-and-error procedures during manufacturing.

In this thesis, a 3-D non-isothermal framework for modeling the VARTM process for a wind turbine blade was developed. The model was utilized in a case study optimizing inlet gate arrangement, resin temperature, and mold temperature to shorten the filling time. Sequential filling scheme was assumed and different inlet gate arrangements and activation times were used in the first phase of the study. It was observed that, although increasing the number of the inlet gates tends to shorten the filling process, its effectiveness kept decreasing monotonically. The generally observed filling issue was the formation of dry spots in the sandwich region at the bottom of the part. In the sandwich region, the core splits the flow and forms two flow fronts, one on the top and another at the bottom of the sandwich region. The two flow fronts converge right after the core. For some cases, the slow moving flow front beneath the core was not able to reach its way out and converge with the flow front on the top of the core. To overcome the problem, activation of the auxiliary inlet gates located on the top of the core was postponed.

In the second phase of the study, different resin temperatures were used. Increasing the temperature up to 325°K resulted in shorter filling durations while increasing the temperature further produced dry spots beneath the core. From the flow pattern results in non-sandwich areas, it was concluded that resolving the issue of slow moving flow front at the bottom of the core

makes it possible to decrease the filling time by 17% through increasing the resin temperature by 20°C. The effect of different mold temperatures on the filling time was examined in the third phase of the study. Increasing the mold temperature from the initial value (330°K) did not result in shorter filling times.

To investigate the necessity of employing 3-D non-isothermal model, a 2.5-D non-isothermal model and a 3-D isothermal model were developed and their results were compared to the results of the 3-D non-isotheral model. The 2.5-D non-isothermal model was unable to accurately predict the flow behavior in the sandwich region. In addition, although the same inlet arrangement and activation times were used for all simulations, the predicted filling time using the 2.5-D model was 30% shorter than the filling time using the 3-D non-isothermal model. On the other hand, the predicted flow pattern for the 3-D isothermal model was very similar to that for 3-D non-isothermal model and the difference between the filling times was relatively small. However, since the model does not keep track of the temperature variations and curing during filling, the simulation of cure after the filling would not provide accurate results.

TABLE OF CONTENTS

TABLE OF CONTENTS (continued)

Chapter Page

LIST OF TABLES

LIST OF FIGURES

LIST OF FIGURES (continued)

Figure Page

CHAPTER 1

INTRODUCTION

Composite materials with their exceptional mechanical properties offer a diverse alternative to the traditional structural materials like steel and aluminum. Advanced composites started to draw attention from the 1960's after the introduction of polymeric composites, but in the recent years, the growth rate in utilizing these materials has been rapidly accelerated in many industries such as marine, aerospace, automotives and energy. One important application of composites is in the wind blade industry where their high stiffness and stiffness to weight ratio made them the material of choice.

This increase in performance does not come cheap, and the sum of material and manufacturing expenses made advanced composites costly. Although the high cost has been tolerated by the aerospace industry, it is a different story for the wind blade manufacturing where the price of wind blades for each unit is limited to less than $200 per kilowatt for it to be economical. Therefore, two approaches have been followed simultaneously by the industry to reduce the costs: (1) Develop lighter, simpler designs that result in more durable parts, (2) Lower the manufacturing costs by developing new processes and increasing the number of produced units [1]. Consequently, the demand for rapid production rates pushes the manufacturers to replace the time-consuming and labor-intensive hand lay-up technique with new automated and faster manufacturing methods.

Vacuum-Assisted Resin Transfer Molding (VARTM) is one of such methods. The process was first employed in 1994 to laminate boat hull structures [2] and has become a widly used and rapidly growing manufacturing method in the wind blade industry [3]. In the VARTM

process, layers of dry fiber are layed on a single-sided mold and then covered with a transparent vacuum bag. Vacuum is applyed to the preform under the bag which, due to the pressure diffrence with the ambient air, works as a motivating force to drive the resin into the preform; it also works as a compaction force which results in desirable fiber volume fraction of the part. The vacuum is retained under the bag, long after the filling stage was completed and until the resin is fully cured.

The VARTM process offers numerous advantages such as: (1) Low tooling cost due to the use of a single side mold, (2) Potential for fabricating large parts with high fiber volume fraction (60-70%), (3) The transparent vacuum bag allows the observation of the filling front which helps in production of defect-free parts, (4) Produces much less scrap comparing to other methods, (5) Low emission of volatile chemicals [4].

Beside all the advantages, VARTM has to offer, it faces some inevitable disadvantages. The complex preform geometry makes it relatively hard to predict the flow pattern and the flexible nature of the vacuum bag makes it difficult to control the final thickness of the preform. Due to these complexities, process design based on trial-and-error is considered expensive and inefficient. In production of small parts manufactured in great numbers, achieving the successful arrangement by losing of a few trial parts can be tolerated. However, in the case of wind blades that large parts are produced in a few numbers, trial-and-error results in excruciating costs.

In process design of the filling process, the parameters have to be defined in a way that ensures a complete impregnation of the preform in the shortest time. Formation of dry spots must be carefully avoided since they can become the crack initiation sites and result in early failure of the part when they are in service. The other important consideration is that the gelation of the resin should not start while the resin is filling the preform, because the resulting increase in resin

viscosity can lead to incomplete filling of the part. In the curing stage, a full conversion of the resin is desired while excessive temperatures has to be avoided since it can lead to resin deterioration, and part distortion. All of these concerns support the fact that especially for large and thick parts, accurate computer models are vital to a successful design of the process parameters.

Numerous models have been developed by researchers to simulate the VARTM process [5-9]. However, there have not been many previous studies particularly in modeling the VARTM process for wind blades. In a thesis done by Koefoed [10], a framework for modeling the VARTM process for a wind blade was established. The model was able to predict the flow pattern through 2-D isothermal filling simulations while the effects of resin curing during filling were neglected. In order to observe the flow pattern in the thickness direction, separate simulations were carried out for each cross section at the points of interest. Due to the isothermal nature of Koefoed's model, it cannot be used for conditions that temperature variations and resin curing during filling affect the flow behavior. Also because of the 2-D nature of the model, it is unable to reveal the total aspects of the flow pattern.

Within this thesis, PAM-RTM modeling package was utilized to simulate the VARTM process for a wind turbine blade and the following objectives were pursued: (a) developing a 3-D non-isothermal filling and curing model for a wind blade, through integrating cure kinetic model, viscosity model, and heat transfer model to the flow model (b) utilizing the 3-D non-isothermal model in a case study with the goal of shortening the filling process, (c) simulate the flow pattern, resin curing, and temperature distribution during and after filling, using the selected parameters obtained in the case study, (d) conducting 2.5-D non-isothermal filling simulation using the selected parameters and compare the results with that of the 3-D non-isothermal

simulation, (e) conducting 3-D isothermal filling simulation using the selected parameters and compare the results with that of the 3-D non-isothermal simulation.

CHAPTER 2

GENERAL BACKGROUND

A composite material is the combination of two or more distinct materials where typically the properties of the combination exceed the properties of its constituents. Generally composites are formed by a reinforcement material embedded within a matrix. The reinforcement part can be fibers or particles and the matrix part can be plastic, ceramic or metals [11].

Fiber reinforced polymers are being increasingly used in different industries for structural applications. These materials have started a revolution among the high performance structures. They offer significant superiority in terms of strength, stiffness and weight reduction, but apart from that, the freedom of changing the fiber direction according to the needs provides the ability of not only design the structure but also design the material at the same time [12].

The functions of the polymeric matrix and the fiber in structural polymeric composites are explained bellow.

Functions of the fiber:

- From 75 to 90% of the loads are carried by the fibers.
- Fibers provide the structural properties such as strength, stiffness and thermal conductivity.
- The fiber direction accounts for electrical conductivity or insulation of the composite.

Functions of the matrix:

- Matrix transfers the load to the fibers through the interfacial bond; avoids fiber- buckling and provides the rigidity of the part.
- Provides chemical and wear protection of the fibers against the environment.

- Isolation and separation of fibers to stop crack propagation.
- Provides the outer shape and appropriate surface finish of the part.
- Properties of the matrix accounts for the impact strength and the ductility of the composite [11].

2.1 Reinforcement Materials

Figure 2.1 shows the specific strength and specific modulus of different fiber reinforced material in comparizon with traditionaly used metals.

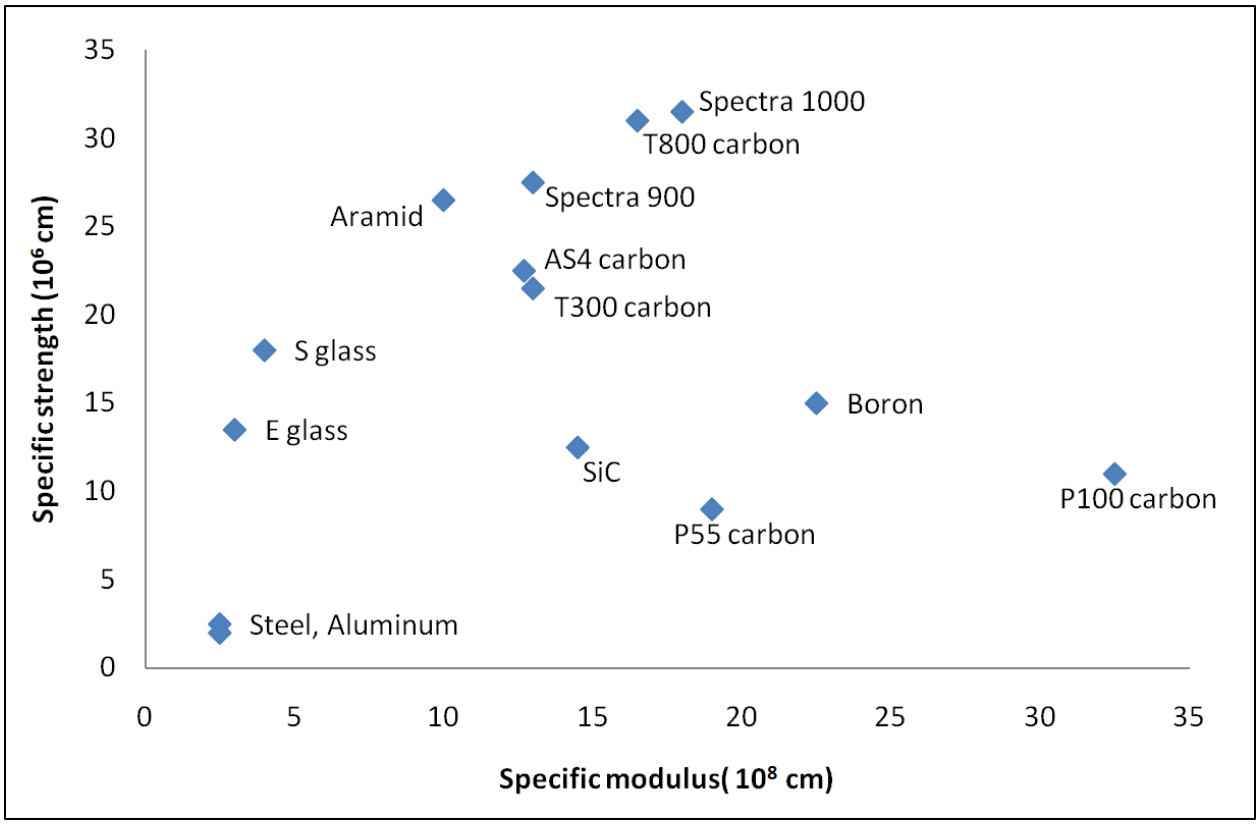

Figure 2.1. Specific strength and specific modulus of fibers and metals [12].

Although Figure 2.1 shows the outstanding superiority of the advanced fibers, other facts must be considered in order to compare them with metals. Fibers can only be utilized in combination with a matrix. The matrix proportion of the composite is in the order of 40% by

volume, and for the case of polymeric composites their strength and stiffness is much lower than the fiber. Furthermore, the properties shown in the Figure 2.1 are for the case of unidirectional fibers, while in reality, for most parts a proportion of the fibers has to be aligned in directions other than the main direction to overcome loads in other directions.

Experiments show that considerable mechanical advantages can still be achieved and aerospace industries have proven it by delivering almost 30% weight reduction in their new products [12]. Table 2.1 shows a list of various types of fibers used in the industry with the asocciated mechanical properties.

TABLE 2.1

MECHANICAL PROPERTIES OF TYPICAL FIBERS [13].

Fiber	Fiber Diameter (μm)	Fiber Density		Tensile Strength		Tensile Modulus	
		(lb/in3)	g/cc	ksi	Gpa	(Msi)	(Gpa)
E-glass	8-14	0.092	0.54	500	3.45	10.5	72.4
S-glass	8-14	0.090	0.49	665	4.58	12.5	86.2
Polyethylene	10-12	0.035	0.97	392	2.70	12.6	87
Aramid	12	0.052	0.44	525	3.62	19.0	130
T300 carbon	7	0.063	0.76	514	3.53	33.6	230
AS4 carbon	7	0.065	0.80	580	4.00	33.0	228
IM7 carbon	5	0.065	0.80	785	5.41	40.0	276
XUHM carbon	------	0.068	0.88	550	3.79	62.0	428
GY80 carbon	8.4	0.071	0.96	270	1.86	83.0	572
Boron	50-203	0.094	0.60	500	3.44	59.0	407
Silicon Carbide	------	0.115	0.19	220	1.52	70.0	483

2.1.1 Glass Fiber

Glass is commonly a composition of SiO2, Al2O3 and some amount of other oxides. Glass fibers are usually produced by pulling and spinning of molten glass. Among the different types of these fibers, E-Glass is the most widely used material amongst the reinforcement materials [14]. Glass reinforced plastic or GRP is a relatively high strength composite with a

reasonable cost. This makes GRP the material of choice for the economically constrained wind blade industry.

Glass in its bulk form has a very low fracture resistance. The great difference in mechanical properties between bulk glass and fiberglass lies on the effects of structural flaws and fracture propagation. Depending on the manufacturing process the number of flaws reduces dramatically for the fiber form, and by reducing the diameter of the fibers the material gets more ductile. When the fibers are incorporated in to composite form, each fiber becomes isolated by the surrounding matrix and even if a single fiber cracks, the fracture would not propagate. Along with all the advantages, the main disadvantages of using GRP can be divided in to two: relatively low modulus, and high density. To overcome the drawbacks, for the case of large wind blades utilizing hybrid structures has been practiced. Using carbon fiber spar caps in combination with glass fiber shells has become a common structure for the offshore wind blades [15].

2.1.2 Carbon Fiber

Carbon fiber as a high performance and lightweight material is being used in a variety of industries. Depending on the processing method and the variables, different properties is achievable with a tradeoff between having high modulus and high strength. High modulus/low stiffness carbon fiber is made out of petroleum pitch with relatively low cost; the intermediate modulus/high stiffness carbon fiber in the other hand is generally made from Polyacrylonitrile (PAN). In Both methods, the precursor is heated and then stretched to form fibers and then the non-carbon materials are removed.

The outstanding strength to weight and stiffness to weight ratio of this material made it a key structural material for high-tech industries. Carbon fiber has obvious mechanical advantages over the traditionally used glass fiber; it has three times the modulus and half the density,

however, the higher costs of the material and also the processing complications made it the second most used material by the industry after glass fiber [16].

In the wind industry, the bulk replacement of glass fiber with carbon fiber is not currently practical. E-glass is produced by cost of almost 2 $/Kg while the production cost of carbon fiber is at least 18 $/Kg [15]. However, as the blades are getting bigger and heavier, the exclusive use of glass fiber as the reinforcement is not practical either and some blade manufacturers have practiced the selective use of carbon fibers for some areas of the blade. The resulting hybrid structures have proven to have superior performance over the traditional glass fiber blades [17].

2.2 Matrix Materials

The polymeric matrix materials are classified into two major categories as thermo-plastics and thermosets. The manufacturing process is quite different for the two categories. Thermoplastics will have to be heated to an elevated temperature and then depending on the process it will be combined with the reinforcement material and then solidifies by simply cooling down. This process is reversible and if the part is heated again the plastic softens and can be deformed; this is an advantage if any repair or rework is needed.

Thermosets in the other hand undergo a curing cycle for solidification, and once it happens they cannot be melted again. During the curing process, molecule chains start connecting each other forming a 3D network. The higher the number of these connections or so called cross-linkings, the more solid and thermally stable the matrix will be. Unlike thermoplastics, which require special considerations with their elevated temperatures, thermoset resins are in the liquid form at room temperature hence are easier to process and can better impregnate the fibers.

Thermosets are more brittle in compare to thermoplastics but they provide better rigidity, greater thermal stability and also high resistance to solvents and chemicals. Table 2 helps to compare a number of thermoset and thermoplastic polymers in terms of mechanical properties.

TABLE 2.2

MECHANICAL PROPERTIES OF TYPICAL RESINS [11].

Resin	Density	Tensile Strength		Tensile Modulus	
	g/cm^3	10^3 psi	(MPa)	10^6 psi	(GPa)
Epoxy	1.2-1.4	7.2-16	50-110	0.36-0.7	2.5-5.0
Polyester	1.1-1.4	5-13.8	35-95	0.23-0.6	1.6-4.1
Phenolic	1.2-1.4	5-9	35-60	0.4-0.6	2.7-4.1
Nylon	1.1	8-13	55-90	0.2-0.5	1.3-3.5
PEEK	1.3-1.35	14.5	100	0.5-0.6	3.5-4.4
PPS	1.3-1.4	11.6	80	0.49	3.4
Polyethylene	0.9-1.0	2.9-5	30-35	0.1-0.2	0.7-1.4
Teflon	2.1-2.3	1.5-5	10-35	-------	-------
Acetal	1.4	10	70	0.5	3.5

2.2.1 Polyester

Unsaturated plyeser resin (UPR) is obtained by reaction of organic acids with an alkohol. The resulting resin has to be mixed with a monomer such as Styrene, so the cure can take place. UPR is the most utilized matrix material by the composite indusry, and represents almost 75% of the total resin used [18]. polyester resins have low cost, low viscosity(better impregnation), low temperature curing, and excelent corrosion resistance. The most significant desadvantage of polyester is the relatively high volumetric shrinkage during the curing process. As the blades are growing in size and weight, manufacturers prefer to use the higher quality and more expensive epoxy resins as the matrix [12].

2.2.2 Epoxy

The epoxy resin is a versatile thermoset widely used by the industry. Although it has a considerably high price but many blade makers found it a good alternative over the traditionally used polyester. Because of its superior mechanical properties, designers have been able to decrease the part's weight significantly.

In addition to the great strength characteristics of epoxy, the processing advantages are countless. Unlike polyester, epoxy shows very small shrinkage during cure, and does not emit volatiles. For the curing, a very wide variety of materials with different proportions can be mixed with the epoxy to achieve the desired property, and curing can take place in a wide range of different temperatures and profiles to achieve different mechanical properties for the product [19].

2.3 Sandwich Materials

The size of wind blades is continuously increasing by the industry. Blade sizes over 60 meters in length have already been installed for 5MW output power. This number is expected to go over 90m in a decade for off-shore wind turbines[20]. As the blades increase in the size, large panels of their structure such as the shell, spar webs and spar caps will be more prone to buckling. Sandwich concept is one efficient way to avoid local buckling by increasing the thickness of the skin and therefore improving the flexural rigidity [21].

Sandwich structure is generally considered as a special type of composite where a thick lightweight core material such as wood or foam is sandwiched between two layer of thin but dense and strong material. Such structure is an excellent way to create a lightweight structure with high bending strength and buckling resistance. The common core materials include Balsa wood, PVC foam, BMI foam and honeycomb [20].

2.4 Vacuum-Assisted Resin Transfer Molding Process

Vacuum-Assisted Resin Transfer Molding (VARTM) has drawn the focus of many wind blade manufacturers. VARTM is a variety of the RTM process and was developed to reduce the design difficulties and the cost of tooling. Instead of two half-molds, it uses one half-mold at the bottom and a vacuum bag on top of the part and therefore the tooling expenses are reduced dramatically [17].

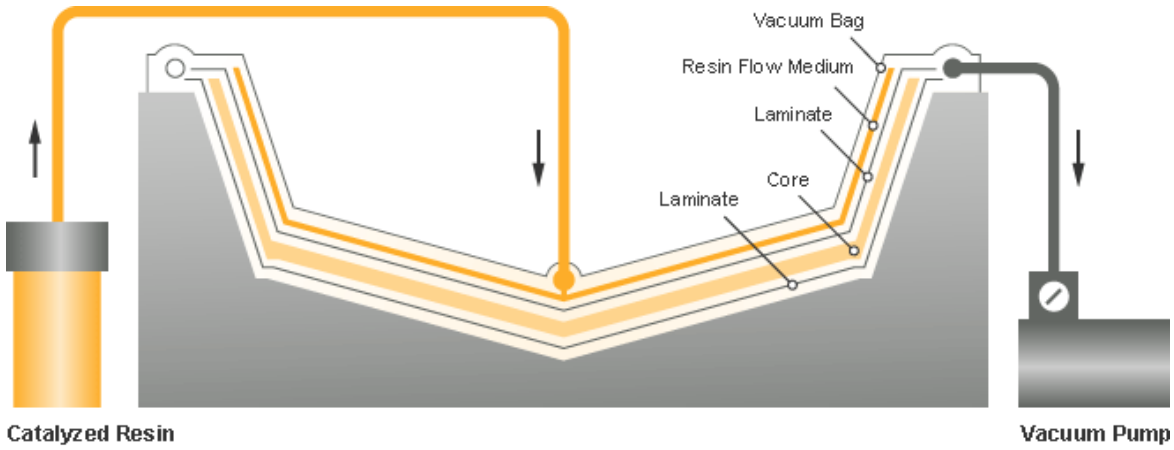

Figure 2.2. Schematic of the VARTM setup [22].

Initially, the vacuum pump sucks the air out of the preform and compresses the fiber layers. At this time, the inlet gate opens and the resin flows in. The pressure difference of 1 atm, not only provides the driving force for the resin to impregnate the fiber, but it also works as the compression force to compact the layers of the preform and increase the fiber volume fraction. The vacuum pump remains working until the part is completely impregnated by the resin. Depending on the resin properties, the part can then be cured at room temperature or at elevated temperatures using an oven. The injection pressure is limited to 1 atm, therefore a high permeability medium is regularly placed on the top of the preform or integrated into the vacuum bag to ease the resin flow. Through this layer the resin rapidly flows in the in-plain direction and distributes on the top of the preform while the bottom layers are still dry. Then the resin flows

downward through the thickness and wets out the bottom layers of the preform. Although the use of permeability media reduces the processing time drastically, for infusion of large parts such as wind blades and boat hulls, other modifications are also required. Since the driving force is limited to 1 atm, the distance that the flow front can reach from one inlet alone is also limited. One common way to overcome the problem is to incorporate several inlets on the top of the part with appropriate arrangement.

2.5 Structure of Typical Composite Wind Blades

There are a wide variety of different methods and structure designs used for wind blades. The general design implemented for the VARTM process by many manufactures, typically consists of two outer shells bonded from the edges with a spar web bonded to the inner surface of both shells [10].The components are manufactured separately by VARTM and then assembled using adhesive and bonding agents to form the final part.

The outer shells not only provide the aerodynamic surface but they also carry most of the load. The spar webs (vertical plates) and the spar caps (horizontal plates) together act as an I-Beam (see Figure2.3) which provides bending strength by taking care of the shear forces.

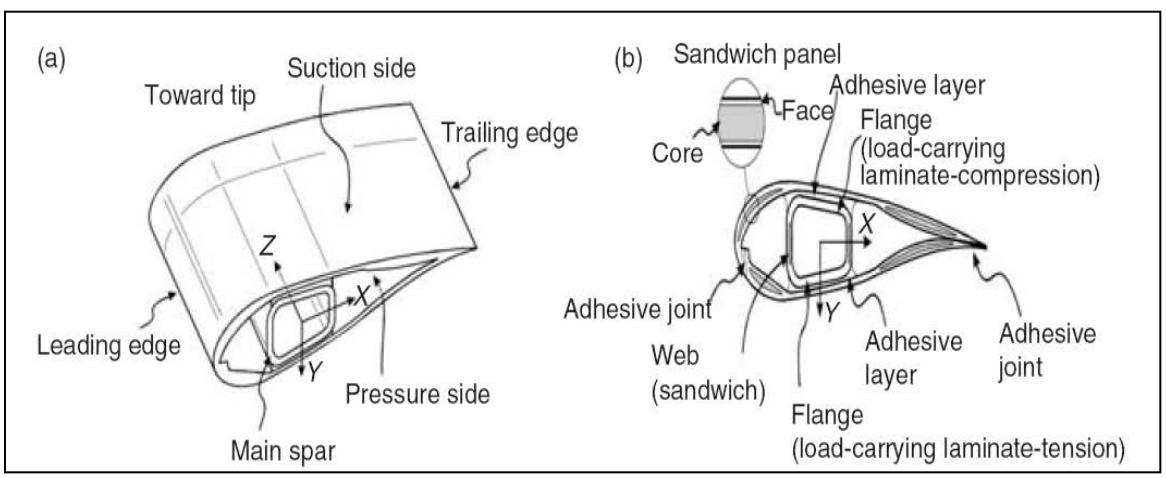

Figure2.3. (a) Placement of outer shells and spar of a wind turbine blade, (b) Detailed cross section view of a wind blade [20].

The first step of the manufacturing process for a wind blade is to cut and prepare the material including different layers of fiber and the core material. The core material is usually closed cell PVC foam or coated balsa wood. The reason for coating the balsa or using close cell foams is to avoid resin to penetrate into the core and increase the overall weight of the part.

The prepared material are then draped and laid up in the mold. Initially a high quality resin called gel coat is applied to the mold. This will result easy release of the part and it also avoids the exposure of dry fibers on the surface of the blade. After gel coat spraying, the material is carefully stacked in to the mold. The structure of the fiber may distort to some extent to adopt curvatures of the mold; this is called draping. Draping has to be done with absolute care to avoid wrinkles, which can dramatically decreases the mechanical properties of the final part [23].

The third step is the preparation for the injection stage. The preform is first covered with a thin textile layer called peel ply; this layer makes it possible to easily separate the injected preform from the vacuum bag and inlets. Then the inlet gates and outlet vents are positioned on the preform. Usually for a large part like a wind blade several inlet lines are placed in the longitudinal direction which will activate sequentially. Finally, all the preform is covered with a vacuum bag and the edges are sealed.

By applying vacuum to the outlet vents, the air is sucked out of the preform and the pressure difference between the atmosphere and under the vacuum bag, forces the preform to compress. After the system was stabilized, the first inlet gate opens and the injection stage initiates.

CHAPTER 3

PROCESS MODELING LITERATURE REVIEW

Producing a satisfactory part using VARTM process is a challenging task. Due to the complications associated with the flexible vacuum bag, and the compaction of the preform makes it very difficult to predict the flow front during resin infusion. The common way for industry to deal with the issue is to let the designing in to hands of experts who heavily rely on experience. Trial-and-error can also help eliminating the problems with inlet/outlet positioning and temperatures. However, this may only be useful for manufacturing relatively small parts; the costs for material loss can be tolerated as long as the redesigning of the mold is not required. For large parts such as boat hulls or wind blades on the other hand, the cost of trial parts is excruciating. Therefore, the employment of modeling tools has become a necessity for large composite part manufactures, to increase the design speed and reduce the costs [24].

A commercial simulation package PAM-RTM developed by ESI group has been successfully used to model complex 2D and 3D parts since 2002. Industries taking advantage of this software are typically the producers of large or complex parts such as energy and marine. It has the ability to model the viscosity effects of curing during the infusion and to simulate curing during and after resin infusion. One advantage of this software is that it allows the user to develop complex parts using graphical software such as CATIA. Besides the meshing abilities that the software has on its own it can also use a finite element mesh generated by other software such as PATRAN or CATIA [25].

3.1 Continuity Equations

A set of differential equations called continuity equations define the transport of a conserved quantity. Since mass, momentum and energy are conserved quantities a wide area of physics can be described by continuity equations.

Mass continuity equations:

$$\frac{D\rho}{Dt} + \nabla \cdot (\rho\vec{v}) = 0 \tag{3.1}$$

Where: $\vec{v}$ is velocity, ρ is density and t is the time

for the case of incompressible fluids such as resins the first term vanishes:

$$\nabla \cdot \vec{v} = 0 \tag{3.2}$$

3.2 Darcy's Law

The Darcy's law [26] describes how the flow rate of a fluid through porous media is related to viscosity, distance, pressure difference, and permeability. It has numerous practical applications in the field of hydrology and fluid dynamics. Darcy's law is also used to model the flow of resin through fabric for numerous composite manufacturing methods [27].

Although the determination of Darcy's law was originally done through experiments, it has also been derived from Stokes steady equation via volume averaging or so-called homogenization.

Darcy's equation:

$$u = -\frac{K}{\mu}\nabla p \tag{3.3}$$

u is called filtration velocity or Darcy's flux which is defined as the volumetric flow per unit area. The actual fluid velocity in a tube packed with a porous material is the volumetric flow rate divided by the tube's cross sectional area thus the actual velocity through the porous media

is obtained, dividing Darcy's flux by the proportion of empty space of the porous media called porosity. Therefore, the modified equation for one-dimensional flow yields

$$v = -\frac{K}{\mu\Phi}\frac{dp}{dx} \tag{3.4}$$

where V is the actual velocity of the fluid in the x direction and Φ is the porosity.

Permeability K is a physical property of the fiber and defines the fluid filling feasibility of the porous media. Permeability is a second order tensor. The general form of the permeability tensor for an arbitrary coordinate system is a 3 by 3 symmetric tensor having six different components. Furthermore, the permeability tensor has only three different components if the orthogonal coordinate system is aligned with the principal directions of the preform structure. In the following equation, K_A and K_P are the permeabilities for arbitrary and principal coordinate systems respectively.

$$K_A = \begin{bmatrix} K_{xx} & K_{xy} & K_{xz} \\ K_{yx} & K_{yy} & K_{yz} \\ K_{zx} & K_{zy} & K_{zz} \end{bmatrix} \quad K_P = \begin{bmatrix} K_{xx} & 0 & 0 \\ 0 & K_{yy} & 0 \\ 0 & 0 & K_{zz} \end{bmatrix} \tag{3.5}$$

Figure 3.1 illustrates the principal permeabilities in an orthogonally layered preform.

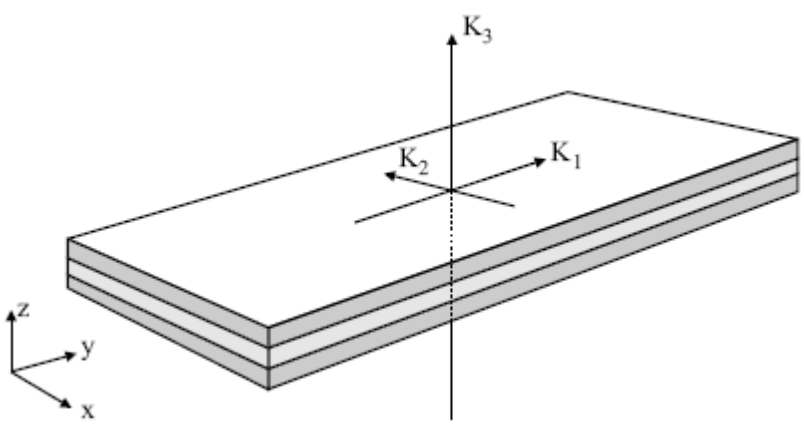

Figure 3.1. Principal permeability directions [10].

3.3 Permeability Determination

One important step for simulating the filling process using Darcy's equation, is determining the permeability tensor. The most accurate and reliable method to determine permeability is through testing. By obtaining resin viscosity, pressure difference and resin velocity the permeability can be calculated. Although it is difficult to calculate the permeability by only having the geometric characteristics of the fabric, some complex micro-models have been used to estimate it. These numerical methods have varying accuracy and in addition, some experiments may still be necessary to determine some of the input parameters such as fiber fraction and fiber diameters. Since typically the thickness is relatively small, most of the numerical methods of determining the permeability consider the part as two-dimensional and are not able to calculate the through thickness permeability.

3.3.1 Permeability Averaging

Once the permeability for different materials is determined, the next step is to calculate permeability for a laminate that consists of numerous materials. In the cases of thin laminate in which the effects of through thickness flow are negligible, the preform can be assumed 2D instead of 3D. Therefore, a rule of mixture can be used to average the permeability of different layers for the in-plane flow.

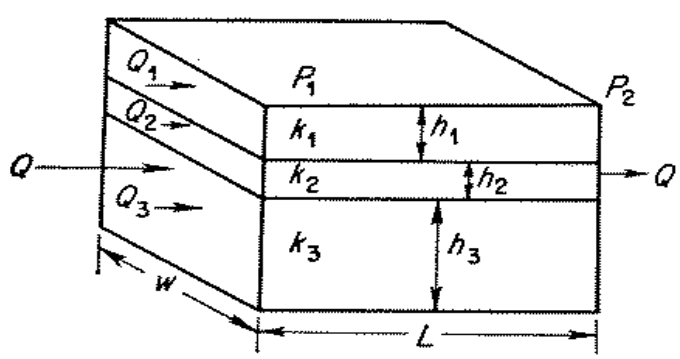

Figure 3.2. In-plane flow into a layered system(parallel flow) [28].

Rearranging (3.13) for the flow rate yields

$$q = \frac{KA}{\mu L}\,\Delta p \tag{3.6}$$

A correct average permeability should result a flow rate equal to the sum of flow rates in every layer [29], therefore

$$q = \frac{\overline{K} w h_{Tot}}{\mu L}\,\Delta p = \frac{K_1 w h_1}{\mu L}\,\Delta p + \frac{K_2 w h_2}{\mu L}\,\Delta p + \frac{K_2 w h_2}{\mu L}\,\Delta p + \cdots \frac{K_n w h_n}{\mu L}\,\Delta p \tag{3.7}$$

Multiplying both sides by $\frac{\mu L}{w \Delta p}$ and rearranging yields

$$\overline{K} = \frac{\sum K_i\, h_i}{h_{Tot}} \tag{3.8}$$

This rule of mixture was evaluated by Diallo et al. [30] for a 40 layer preform and turned to have a close agreement with the experimental results. It was concluded that the stacking sequence influences the accurasy of the model due to effects of numerous interfaces.

For thick laminates produced by liquid composite molding techniques, the flow through thickness is no longer negligible. In order to determine the permeability for the thickness direction it should be considered that the total pressure difference is equal to the sum of pressure differences and the flow rate is identical for every layer of the preform. Figure 3.3 shows the layer arrangement and flow direction.

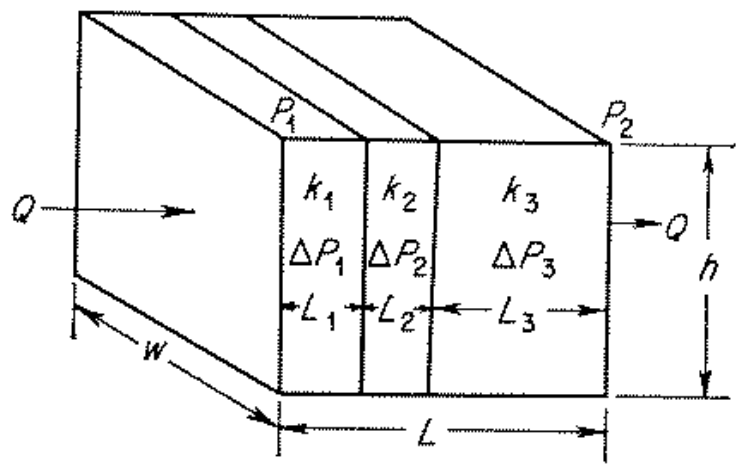

Figure 3.3. Through thickness flow in a layered system (serial flow) [28].

The following equation is valid for the system

$$\Delta p_{Tot} = \frac{q\mu L_{Tot}}{\overline{K}wh} = \frac{q\mu L_1}{K_1 wh} + \frac{q\mu L_2}{K_2 wh} + \cdots \frac{q\mu L_2}{K_2 wh} \tag{3.9}$$

multiplying both sides by $\frac{wh}{q\mu}$ and rearranging yields

$$\overline{K} = \frac{L_{Tot}}{\sum \frac{L_i}{K_i}} \tag{3.10}$$

3.3.2 Experimental Methods

Experimental methods for determining the permeability are more accurate than analytic methods. The existence of different sorts of variations in the real process and also the anisotropic nature of the fibers makes it very difficult to determine the permeability theoretically. Therefore, experimental determination of the permeability based on Darcy's law is the most accurate. For permeability measurement Darcy used a column of sand and measured the flow rate while Δp

was easily calculated from the column's height. By substituting into (3.11) he obtained the isotropic permeability of the particular sand. (3.11) is simply obtained by rearranging (3.3).

$$K = \frac{q\mu}{A}\frac{\Delta L}{\Delta p} \tag{3.11}$$

Equation (3.11) is only utilized for the case of saturated flow. Permeability can either be measured for saturated flow as done by Lundstrom et al. [31] or by the unsaturated flow. In the saturated flow method the initially dry preform are fully saturated and only when a steady state flow was achieved, the flow rate can be measured. Saturated flow method can accurately characterize the permeability but one main shortcoming is that in order to obtain the permeability tensor for anisotropic materials, experiment should be repeated for each direction. In the unsaturated flow method however, the measurements take place while the flow front moves and impregnates the dry preform. Although Gebart [32] and Lai [33] reported same permeability values for the two methods, many other studies indicate that the differences are significant.

There are mainly three experimental methods of measuring permeability for unsaturated flow (moving flow front). They are 1-D linear flow, 2-D radial flow and 3-d hemispherical flow. No matter what method is being used, devices are needed to determine the pressure difference, and the flow rate during the experiment.

3.4 Cure kinetic Modeling of the Resin

One important stage in processing composites using thermoset resins is the curing. Curing is referred to solidifying the monomer or oligomer molecules of a resin through forming a crosslinking network. The reaction can be activated by either heating up or adding an initiator agent. Degree of cure is defined as the fraction of the cross linking network formed. Curing is generally an exothermic reaction and the excessive heat has to be transferred out of the part to prevent deterioration of the polymer.

As the curing advances molecular weight increase and so does the viscosity. At the same time, the released heat tends to decrease the viscosity; this makes it very complicated to predict the flow behavior of the resin. Therefore, cure kinetics characterization of the resin is essential to deal with resin flow and heat concentration issues. The ideal cure kinetic model should be able to describe the changes in the reacting material and at the same time should be simple enough to be linked with a model that simulates flow and curing behavior of the resin during and after the mold filling process.

For estimating the required time for a resin to solidify, a model of reaction rate has to be defined. The following model developed by Kamal and Sourour [34] has become the basis for many studies in resin curing.

$$\frac{d\alpha}{dt} = \left(K_1 + K_2\,\alpha^m\right)(1-\alpha)^n \tag{3.12}$$

$$K_i = A\,e^{\frac{-E_a}{RT}} \tag{3.13}$$

Where $\frac{d\alpha}{dt}$ is the conversion rate, α is the degree of cure and, K_1 and K_2 are rate constants and are obtained from Arrhenius equation (3.13) where **A** is the pre-exponential factor, $\mathbf{E_a}$ is the activation energy, **R** is the ideal gas constant, and **T** is the temperature in Kelvin. Although, Kamal Sourour model is not based on the resin chemistry, it offers adequate precision in terms of temperature profile, overall cure rate, and heat of reaction for many resin systems.

3.5 Rheological Modeling

In liquid composite molding, the resin starts filling the mold at a low viscosity. As the chemical reaction progresses during and after filling, the viscosity increases towards infinity either because of crosslinking or physical changes such as crystallization. During the filling process, it is crucial that the viscosity does not reach a high value before the preform is totally

impregnated by the resin. After filling, the curing stage starts and reaction progresses further until a sufficient mechanical strength is achieved to eject the part from the mold. There are many empirical viscosity models available for different resin systems [35-38]. Most implicated Viscosity models for common thermoset resins describe the viscosity as a function of temperature and degree of cure. By linking the viscosity model with flow model, heat transfer model, and cure kinetic model, accurate prediction of flow pattern in different times can be achieved.

3.6 Isothermal vs. Non-Isothermal Flow Modeling

Non-isothermal flow is referred to the cases in which the temperature changes of the resin is significant during filling [39]. For many cases, the resin enters the mold in temperatures lower than the one of mold. At the start, by the heating from the mold the viscosity of the resin may decrease by orders of magnitude. Later on, the high temperature activates the polymerization reaction, which for exothermic reactions adds more heat to the system. The generated heat tends to decrease the viscosity while at the same time, the formation of crosslinkings works in the opposite direction. Therefore, due to the complex nature of the problem, in order to obtain an accurate prediction of the flow behavior, it is necessary to link heat transfer model, cure kinetic model and viscosity model of the resin to the flow model.

Iso-thermal flow can be assumed where the resin, the mold, and the preform have the same temperature at the start of the filling, and temperature variation is minimal during the filling. Also the effects of curing on viscosity during filling are neglected. The computation time for isothermal simulations is much shorter in compare to the non-isothermal simulations.

CHAPTER 4

WIND BLADE MODEL PREPARATION AND METHODOLOGY

4.1 Geometry and Meshing

The 48 meters long composite blade from TPI Composites was selected for the model; the dimensions are shown in Figure 4.1.

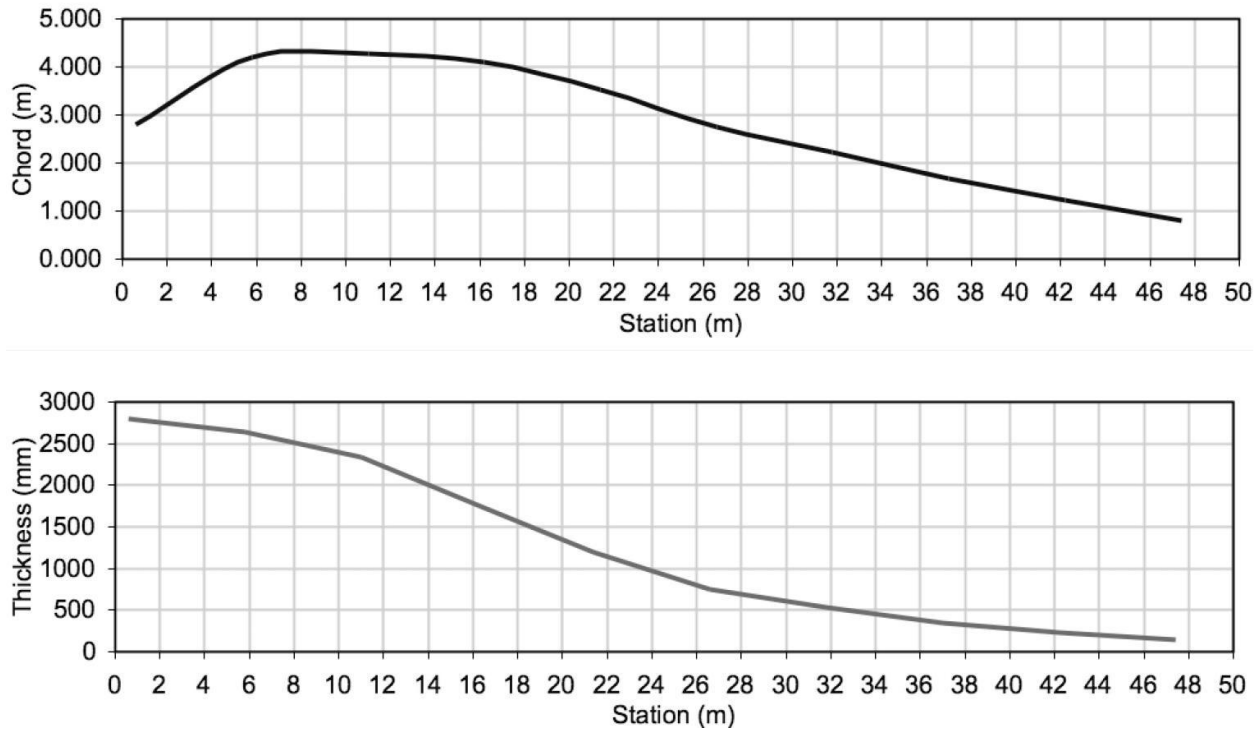

Figure 4.1. Thickness and cord dimensions of the modeled wind blade [40].

The geometry of the blade was created using CATIA. The outer surface of the blade was created by 15 airfoil cross-sections along the blade's shell, and then the “multi-section surface” function was used to create a smooth surface that passes through all indicated cross sections.

Next step was to mesh the surface geometry. The arrangement of the elements at this level is very important because the indication of the inlet gates and vents in PAM-RTM software

takes place through marking the surface of some selected elements. Therefore, to arrange the elements in an appropriate manner it is vital to have a general idea about the shape and the positioning of inlet gates and vents in a real manufacturing scenario.

In production of wind blade shells using VARTM method, the sequential filling scheme is being applied by many of the VARTM wind blade manufacturers. The technique was first presented by Chan and Morgan [41] and includes multiple omega-shape channels that are placed on the top of the part in the longitudinal direction along the blade, while the vacuum outlet lines are positioned at the edges of the preform. As soon as the filling starts, the inlet lines carry the resin along the length of the blade almost instantly and then the resin has a shorter distance to infuse in the transverse direction. Resin injection initially starts from the center inlet line (main inlet gate) and then the other inlets (auxiliary inlet gates) on both sides of the center inlet are activated afterwards as soon as the flow front reaches them. The auxiliary inlet gates would activate one after another until the preform is fully impregnated by the resin (see Figure 4.2).

Another important issue in creating the geometry and meshing is to choose an appropriate number of elements for the model. Although it is beneficial to minimize the number of elements for reducing the computational time, the accuracy of the simulation is lower. Another important fact is that the indication of inlet gate takes place by marking a row of selected element, therefore high number of element rows provides more potential places. This gives more option for determining the number and position of the inlet lines in the process design and optimization step.

Figure 4.2. Filling process of a wind blade shell in TPI Co [42].

In the current study, the idea was to align the elements in the same manner so that each row of elements could be defined as an inlet channel and the elements located at the edges of the model could be defined as the vents. In order to arrange the elements, guiding curves had to be created. The center guiding curve was created through “spline” function, using the geodesic center points of the cross-sections. The rest of the guiding curves were created as offsets from the center curve with 15 cm distance from each other (see Figure 4.3).

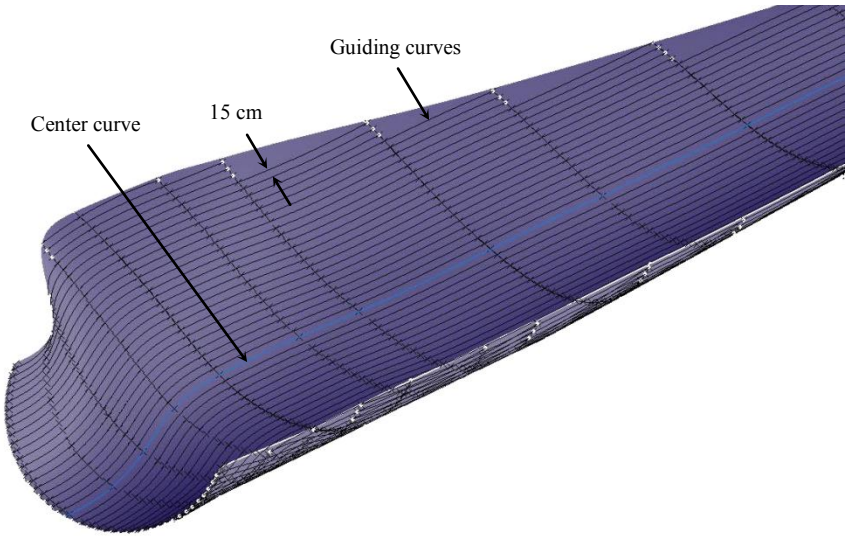

Figure 4.3. Guiding curves for element arrangement.

The geometry was then imported to the “Advanced Meshing Tool” module of CATIA for meshing. The location of the nodes were initiated on the guiding curves before the “meshing” function took place. This was done by using “Impose Elements” function. Once the location of the imposed nodes was identified, “Octree Triangle Mesh” function was applied to the surface geometry to discretize it (see Figure 4.4). The surface mesh was exported as a NASTRAN mesh file to PAM-RTM software for filling and curing simulations. Having imported the mesh the rest of the process was performed in PAM-RTM.

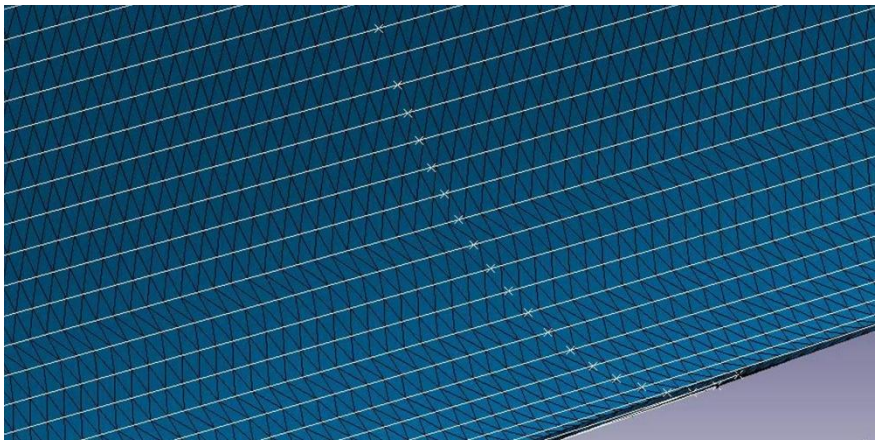

Figure 4.4. Surface mesh of the part.

4.2 Laminates

The preform was assumed to be a lay-up of different layers of glass fiber in combination with balsa wood as the core material. The preform was divided into two main regions: the sandwich laminate region and the main laminate region. In the sandwich region, the balsa wood is sandwiched between layers of glass fiber. The layup arrangement of both laminates is defined in the following paragraph. Figure 4.5 shows the location of the main and sandwich regions. The laminates and their thicknesses are defined as in Tables 4.1 and 4.2.

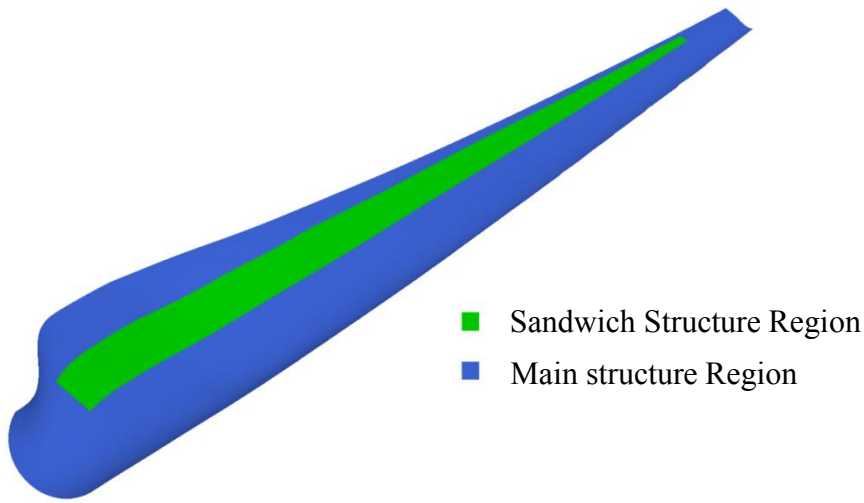

Figure 4.5. Location of the sandwich structure and main structure of the wind blade part.

TABLE 4.1

LAYER THICKNESSES OF MAIN LAMINATE.

Layer1 : Continuous fiber mat (CFM) on top	h_1=10mm
Layer2 : Biaxial fiber	h_2=30mm
Layer3 : CFM at the bottom	h_3=10mm

(CFM: Continuous Fiber Mat)

TABLE 4.2

LAYER THICKNESSES OF SANDWICH LAMINATE.

Layer1 : CFM on top	h_1=10mm
Layer2 : Core material	h_2=20mm
Layer3 : Biaxial fiber	h_3=10mm
Layer4 : CFM at the bottom	h_4=10mm

For 3-D simulations, the "Mesh Extrusion" function was used to create six node prismatic pentahedral elements with respect to layer thicknesses. The permeability orientation for all the laminates was defined as K_1 in the longitudinal direction of the blade, K_2 in the in-plane transverse direction (perpendicular to K_1), and K_3 in the through-thickness direction (see the permeability values in Table4.3).

For 2.5-D simulations, the software calculates a local permeability at every point of the blade by computing the average permeability of the layers placed along the thickness of the part. Figure 4.6 illustrates how the layers of the preform and the core material were positioned.

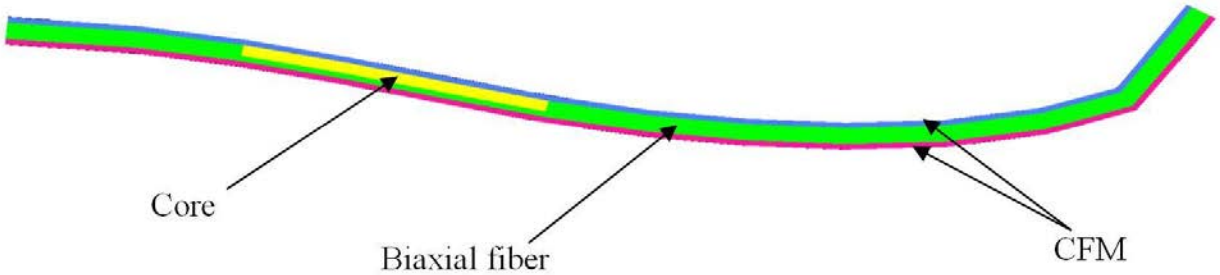

Figure 4.6. Cross-section of the discretized composite wind turbine blade.

4.3 Material Properties

4.3.1 Preform Properties

The permeability and porosity values for different fiber structures were obtained from reference [10] as shown in Table 4.3. Properties of the material used in the preform were obtained from reference [43] and are shown in Table 4.4.

TABLE 4.3

PERMEABILITY AND POROSITY VALUES OF DIFFERENT FIBER STRUCTURES [10].

	Permeability			Porosity
	K1	K2	K3	
Biaxial	1.8 E -11 m3	1.8 E -11 m3	1.1 E -12 m3	0.5
CFM	1.6 E -9 m3	1.6 E -11 m3	5.44 E -11 m3	0.8

TABLE 4.4

MATERIAL PROPERTIES OF THE PREFORM [43].

	Density	Specific heat	Thermal conductivity
Glass fiber	2480 Kg/m3	740 j/Kg.K	1.3 W/m.K
Balsa	150 Kg/m3	2900 j/Kg.K	0.06 W/m.K

4.3.2 Resin Properties

The resin was assumed to be non-thixotropic and the injection process was assumed to be non-isothermal for the case study. The catalysts were assumed to be mixed with the resin on-line and right before entering the part.

For the non-isothermal filling simulation, two main models were incorporated: (1) a cure kinetic model for modeling the curing and heat generation behavior of the resin, and (2) a viscosity model to model the viscosity as a function of degree of cure and temperature.

4.3.2.1 Cure Kinetic Model for Polymerization

The model selected to simulate the curing kinetics is the Kamal-Sourour model [34]. The Kamal-Sourour equation for a resin with n components is as follows:

$$\alpha = \sum_{i=1}^{n} c_i \, \alpha_i \tag{4.1}$$

$$\frac{d\alpha_i}{dt} = K_i(T).\alpha^{m_i}.(1-\alpha)^{n_i} \tag{4.2}$$

Where α is the degree of cure, C_i is the weight parameter of each reaction, K_i is the rate constant of the chemical reaction and $\frac{d\alpha_i}{dt}$ is the rate of reaction for the ith component, the values of K_i are defined by the Arrhenius rate law:

$$K_i = A_i \exp\left(-\frac{E_i}{R.T}\right) \tag{4.3}$$

Where A_i are the pre-exponential factors, E_i are the activation energies of the chemical reaction, m_i and p_i are exponents that characterize the sensitivity of each autocatalytic reaction, R is the universal gas constant, and T is the temperature of the system.

Based on the Kamal-Sourour model, Lee and Kim [44] expressed the model for unsaturated polyester resin. This expression takes the effects of added catalysts in to consideration:

$$\frac{d\alpha_i}{dt} = K_i\,(T)\,[MEKPO]^p.[Co.Na]^q.\alpha^{m_i}.(1-\alpha)^{n_i} \tag{4.4}$$

Where MEKPO is the initiator additive Methyl Ethyl Ketone Peroxide and Co.Na is the accelerator additive Cobalt Naphthenate. The kinetic parameters of the unsaturated polyester resin were obtained from reference [44] and are shown in Table 4.5.

TABLE 4.5

PARAMETERS OF THE KINETIC MODEL.

A (s^{-1})	$\frac{E}{R}$ (K)	m	n	H_r (cal/g)	ρ_r (Kg/m^3)	C (J/Kg.K)	k_r (W/mK)	MEKPO (phr)	Co.Na (phr)	P	q
2.336×10^7	8.354×10^3	0.18	1.82	98.08	1350	1720	0.3	0.5	0.1	1.08	0.29

- A : Pre-exponential factor
- $\frac{E}{R}$: Activation energy
- m : First exponent
- n : Second exponent
- H_r : Enthalpy of reaction
- ρ_r : Density
- C : Specific heat
- k_r : Thermal conductivity
- MEKPO : Amount of the initiator
- Co.Na : Amount of the accelerator
- P : Initiator exponent
- q : Accelerator exponent

4.3.2.2 Viscosity Model

Based on the application of William-Landel-Ferry theory, Han and Lee [45] expressed the following viscosity model for unsaturated polyester resin:

$$\log\mu = \log\mu_{T_g} - \left(\frac{a(T - T_{g)}}{51.6 + T - T_g}\right) \tag{4.5}$$

Lee and Kim [44] measured T_g and a and obtained the following equations:

$$T_g = 209 + 62\alpha + 71.4\alpha^2 \tag{4.6}$$

$$a = 8.27 + 12.17\alpha \tag{4.7}$$

$$\log\mu_{T_g} = 6.01 + 9.54\alpha \tag{4.8}$$

By substituting Equations (4.6), (4.7) and (4.8) in to the Han-Lee model (4.5) yields to:

$$\log\mu = 6.01 + 9.54\alpha \left(\frac{(8.27 + 12.17\alpha)(T - 209 - 62\alpha - 71.4\alpha^2)}{T - 157.4 - 62\alpha - 71.4\alpha^2}\right) \quad (4.9)$$

or

$$\mu = 10\text{^}\left[\left(6.01 + 9.54\,\alpha - \left(\frac{(8.27 + 12.17\alpha)(T - 209 - 62\alpha - 71.4\alpha^2)}{T - 157.4 - 62\alpha - 71.4\alpha^2}\right)\right) - 1\right] \text{ Pa.s}$$

4.4 Thermal Boundary Conditions for Non-Isothermal Simulations

For the non-isothermal filling simulations the assumption is that, the resin is mixed with the curing agent online and injected to the preform. As soon as the resin is injected to the mold, its temperature changes by contacting the mold and the preform, which are at different temperatures. Later on, the resin starts to cure and the generated heat from the chemical reaction transfers by conduction through the part and also by convection with the surrounding air. The areas closer to the edges and tip of the blade were assumed to have a higher convection with the surrounding air than that of the center of the blade, also the entire bottom surface (mold side) was assumed to have a constant convection coefficient (see Figure 4.7).

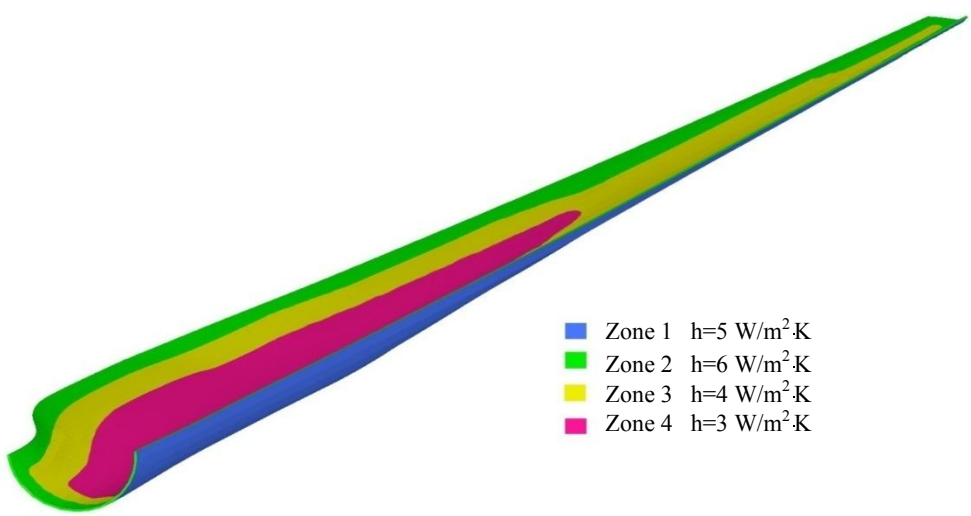

Figure 4.7. Convection heat transfer coefficient for different zones of the part.

CHAPTER 5

SIMULATION RESULTS

Once the model was prepared, the next step was to investigate how process variables affect the wind manufacturing process. The goal was to optimize the process by shortening the injection time. The general format of positioning inlet lines and outlet vents for the model is based on sequential filling scheme (see Figure 4.2). The outlet vents are assumed to be placed on the longitudinal edges of the blade while the inlet lines are positioned longitudinally on top of the part and parallel to each other.

5.1 Case Study and Optimization

5.1.1 Number and Position of the Inlet Gates

In the first phase of this case study, different numbers of inlets in different positions were used. For all cases, the main inlet was placed longitudinally at the center of the part while auxiliary gates were placed on the two sides of the main inlet gate. The number of auxiliary gates, their positions, and their activation times were varied for different cases. The outlet vents were defined on the side edges of the part, similar for all different cases. The mold was assumed to have no heating or cooling capabilities and the initial mold temperature, the initial resin temperature, and the ambient air temperature was assumed to be 330°K, 320°K, and 300°K respectively.

5.1.1.1 Case 1: Single Inlet Gate

For Case 1, no auxiliary inlet gates were considered for the part, so the resin was injected solely through the main inlet gate, indicated by color blue in Figure 5.1.

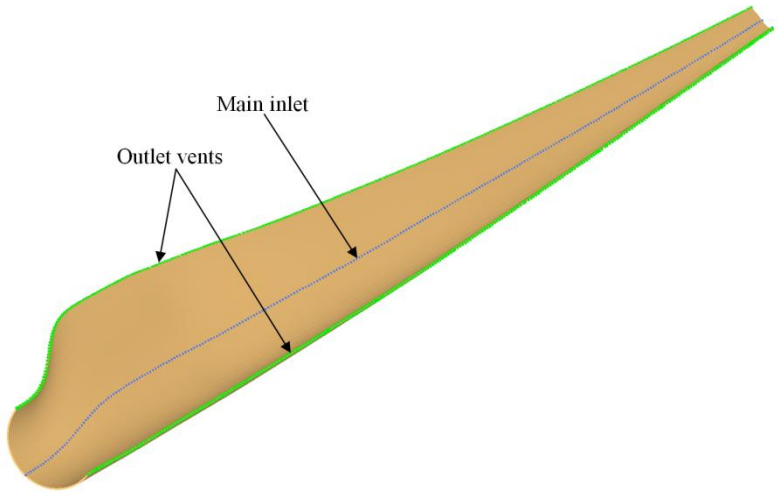

Figure 5.1. Inlet gate and outlet vents positioning for Case 1.

For Case 1, the resin was not able to fully impregnate the preform and the flow stopped at 10,995 seconds after the start of filling (see Figure 5.2). At the beginning of the filling, the flow front remained nearly parallel to the inlet gate. As soon as the flow front entered the sandwich region, the velocity increased on top of the core where only a single layer of CFM exists. The core is impenetrable and there is no flow in the thickness direction, Therefore, the resin flows faster in the in-lane direction. At the bottom of the part, the flow front kept its parallel pattern throughout the filling stage. This is mainly because there is an additional 1 cm thick biaxial layer at the bottom of the core which restricts the flow speed.

The degree of cure of the resin at the end of filling is shown in Figure 5.3. The area containing the core material started curing sooner than the remaining filled portion of the blade. The heat transfer between the resin and the core explains the behavior. Because the core had a 10K higher initial temperature than the resin, it made the neighboring resin warmer and triggered an early curing in that area.

Evidently, the single inlet line failed to fill the preform due to elongation of the filling process and as can be seen in Figure 5.3 the resin had reached a high degree of cure and the resulting high viscosity had totally blocked the flow.

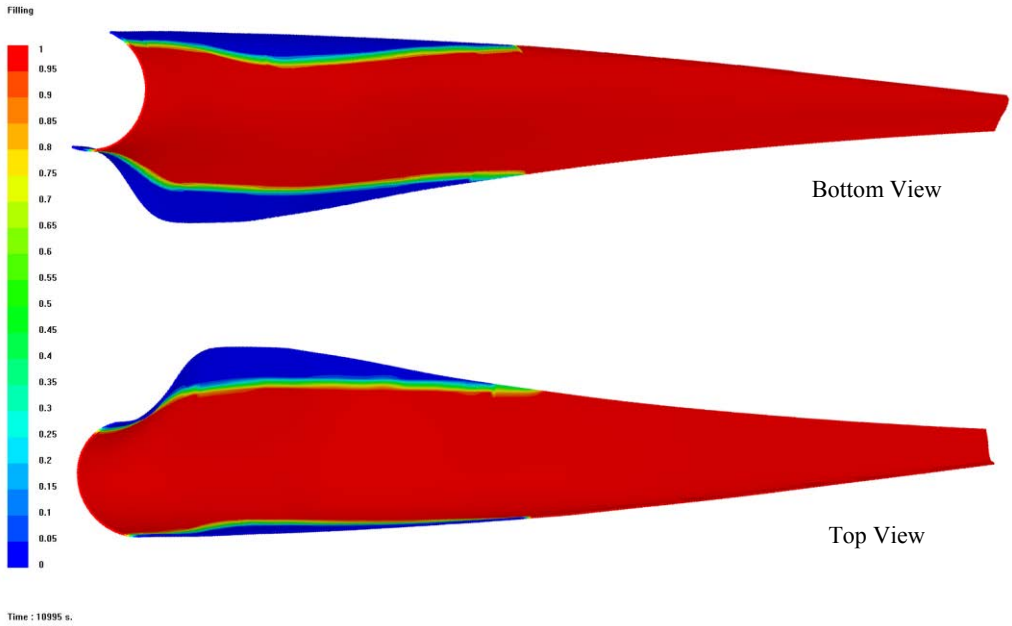

Figure 5.2. Filling pattern for Case 1 at 10,955s (end of filling).

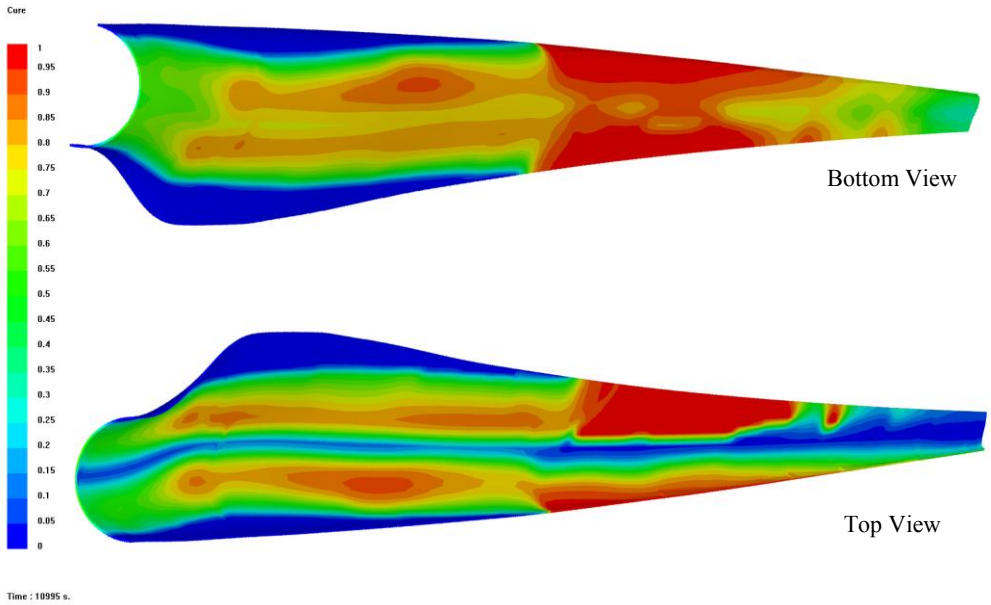

Figure 5.3. Degree of cure for Case 1 at 10,955s (end of filling).

5.1.1.2 Case 2: Three Inlet Gates

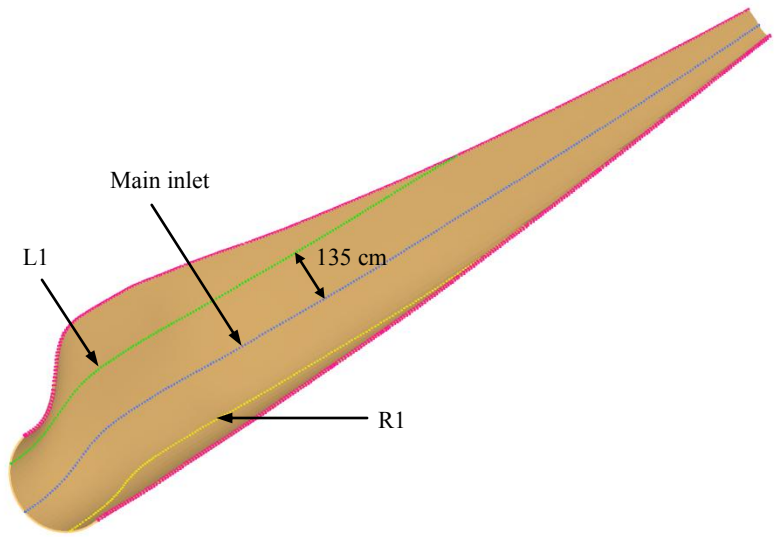

Figure 5.4. Inlet gate and outlet vents positioning for Case 2.

For Case 2, one auxiliary gate was placed on each side of the main inlet gate, half way from the main gate to the outlet vents (edge of the wind blade); the inlet to the right side of the main inlet was named R1 and the inlet to the left side of the main inlet was named L1. In the first attempt, the activation time for both auxiliary gates was chosen to be 2,700 seconds after the start of filling. Figure 5.5 shows the part at the end of filling, in which large dry spots can be observed in the sandwich region at the bottom (mold side) of the part.

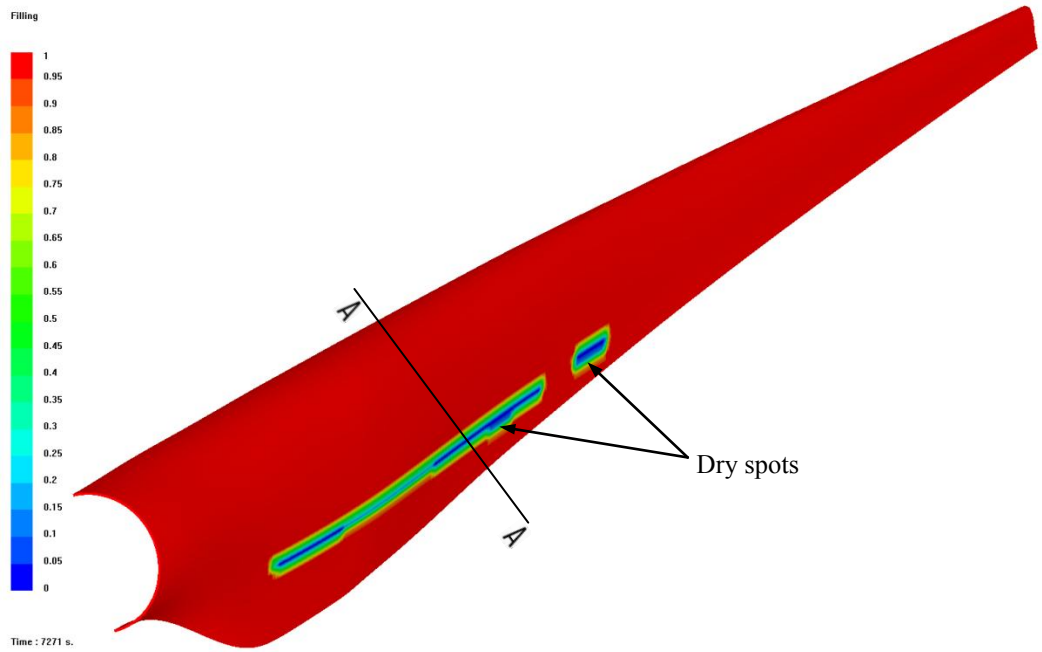

Figure 5.5. Location of the resulting dry spots for the first attempt of Case 2.

PAM-RTM is able to show the flow pattern inside the part by sectioning it at a point of interest. In this case, the part was sectioned by A-A as shown in Figure 5.5. Figure 5.6 shows the structure of the part and also the location of the inlets at section A-A.

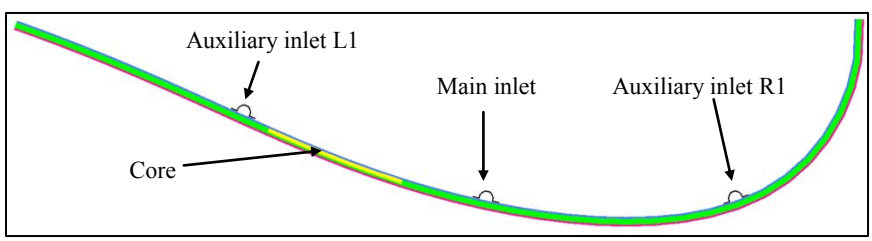

Figure 5.6. Cross section view of core material and inlet positions for Case 2.

As can be seen in Figure 5.7(a), the resin flows faster in the in-plane direction compared to the flow in thickness direction because the in-plane permeability values of all layers are greater than their through-thickness permeability value. As the flow front reaches the sandwich region (in the left side of the main inlet gate), it splits by the core material. Since the core layer is

not permeable, the resin flows separately in the layers on the top and bottom of the core material. The upper flow front is boosted by activation of the auxiliary inlet L1 at 2,700 seconds after the start of the filling process. As soon as the upper flow front passes the core, it starts infiltrating downwards in the thickness direction. Before the lower flow front can reach its way out, the resin from the upper flow front reaches the bottom of the part and blocks the way. This results in dry spot formation beneath the core.

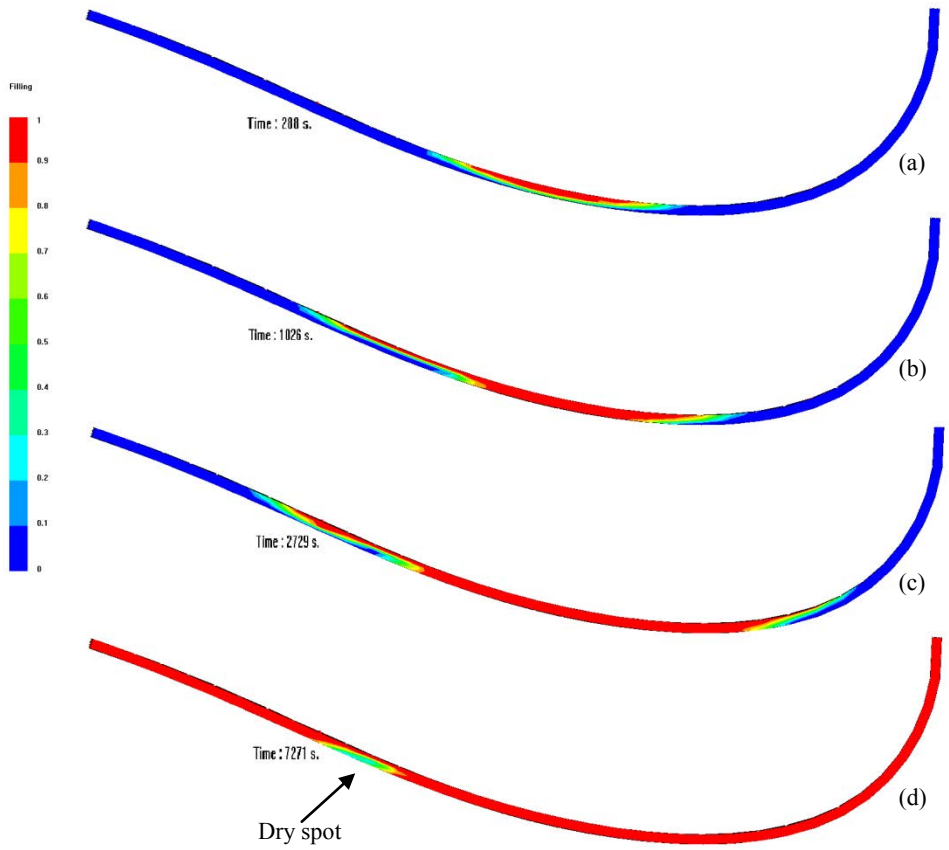

Figure 5.7. Flow pattern at section A-A of Case2.

Apparently, the activation of L1 auxiliary inlet at 2,700 seconds pushed the upper flow front early and caused the formation of dry spots. Therefore, it was concluded that a delay in activation of L1 might provide enough time for the lower flow front to leave the sandwich region on time and converge to the upper flow front without leaving voids. After several trials, the

activation time of 3,400 seconds for L1 resulted in full impregnation of the preform in the shortest time.

Table 5.1 shows the activation times for each of the auxiliary gates. The filling times were calculated separately for the two sides of the main inlet gate.

TABLE 5.1

ACTIVATION TIMES AND FILLING TIMES FOR CASE 2

Inlets	R1	L1	Left side Filling time	Right side Filling time
Activation times [s]	2,700	3,400	8,642 s	7,583 s

5.1.1.3 Case 3: Five Inlet Gates

For Case 3, two auxiliary gates were placed on each side of the main inlet gate, 95cm apart from each other. The location of the inlet gates are shown in Figure 5.8.

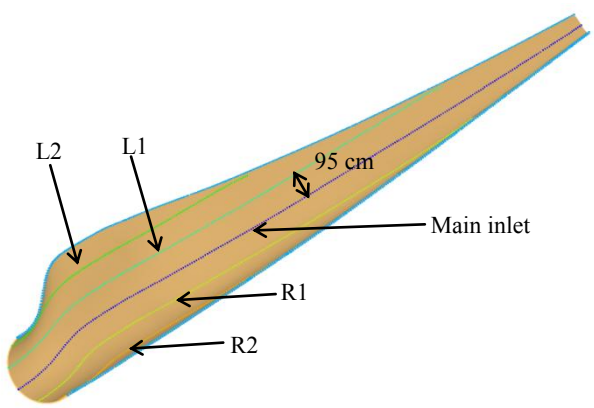

Figure 5.8. Inlet gate and outlet vents positioning for Case 3.

The same problem discussed for Case 2 occurred in Case 3. For the right side of the main inlet gate, when the auxiliary gates were activated, it took 3,902 seconds to fill the preform. For the left side, however, the complications with the sandwich structure required delayed activations of the auxiliary gates. As such, the filling process was longer, taking 5,716 seconds to be completed. Table 5.3 shows the inlet gate activation times and filling times for Case 3.

TABLE 5.2

ACTIVATION TIMES AND FILLING TIMES FOR CASE 3

Inlets	L1	L2	R1	R2	Left side Filling time	Right side Filling time
Activation times [s]	2,200	3,700	1,050	2,150	5,716 s	3,902 s

5.1.1.4 Case 4: Seven Inlet Gates

For Case 4, three auxiliary inlet gates were placed on each side of the main inlet gate. Figure 5.9 shows the location of the inlets. An attempt was made to make the distances between the inlets consistent but the limitation with the mesh did not allow it, therefore, the third auxiliary inlet on each side was placed half way from the second auxiliary gate to the outlet vent.

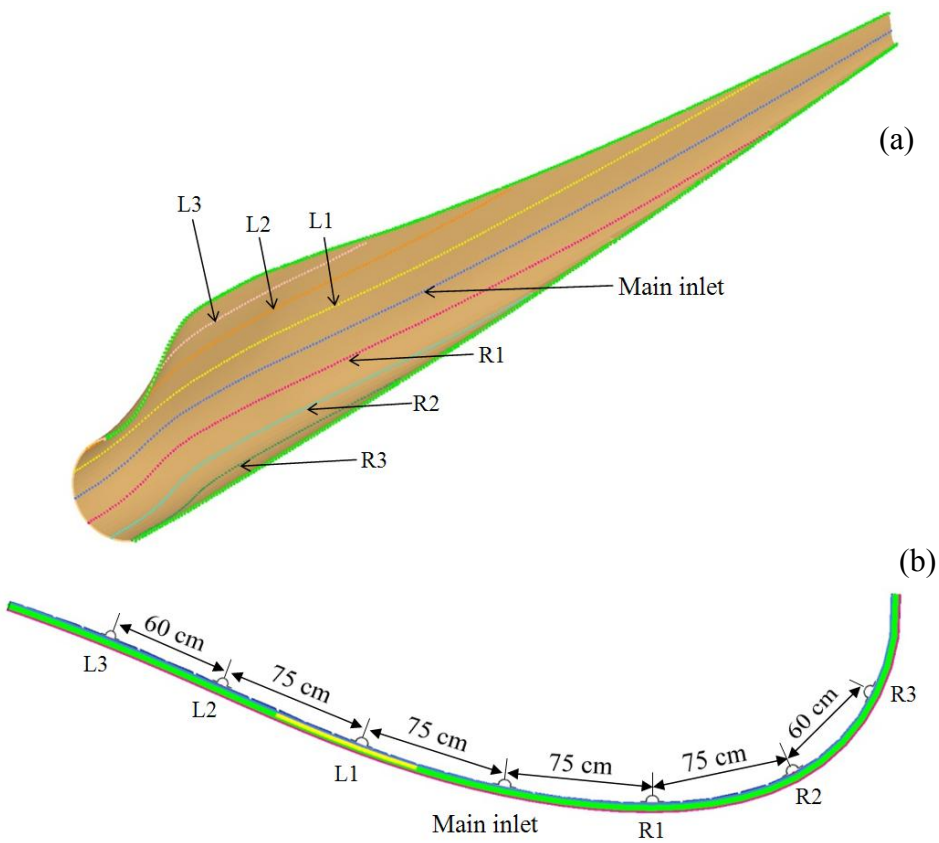

Figure 5.9. (a) Inlet gates and outlet vents positioning for Case 4, (b) Cross section view of the inlet locations.

Different activation times were tried for the auxiliary gates and the combination that resulted in the shortest filling time is shown in Table 5.3.

TABLE 5.3

ACTIVATION TIMES AND FILLING TIMES FOR CASE 4

Inlets	L1	L2	L3	R1	R2	R3	Filling time (Left)	Filling time (Right)
Activation times [s]	1,800	3,200	3,600	650	1,350	1,750	4,614 s	2,571 s

In general, when the main inlet gate activates, the resin flows to both sides of the inlet gate forming two flow fronts moving to opposite directions. Due to the differences in structure and the required activation times on the two sides, the filling times are different for the two sides. In some cases with several auxiliary gates, the filling process in one side may end significantly sooner than the other side. Since the goal is to shorten the overall filling duration, the early impregnation in one side would be pointless; therefore a number of unnecessary auxiliary gates can be removed from that side.

In the recent case, the filling time on the right side of the main inlet is 44% shorter than the left side. As it was shown in Table 5.2, using only two inlet gates on the right side results in a filling time of 3,902 seconds for that side, which is still less than 4,614 second for the left side, therefore, auxiliary gate R3 was considered unnecessary and can be removed.

5.1.1.5 Case 5: Nine Inlet Gates

Four auxiliary inlet gates were defined on each side of the main inlet gate; their locations are shown in Figure 5.10. Different activation times for auxiliary gates were tried. The combination that resulted in the shortest filling time is shown in Table 5.4.

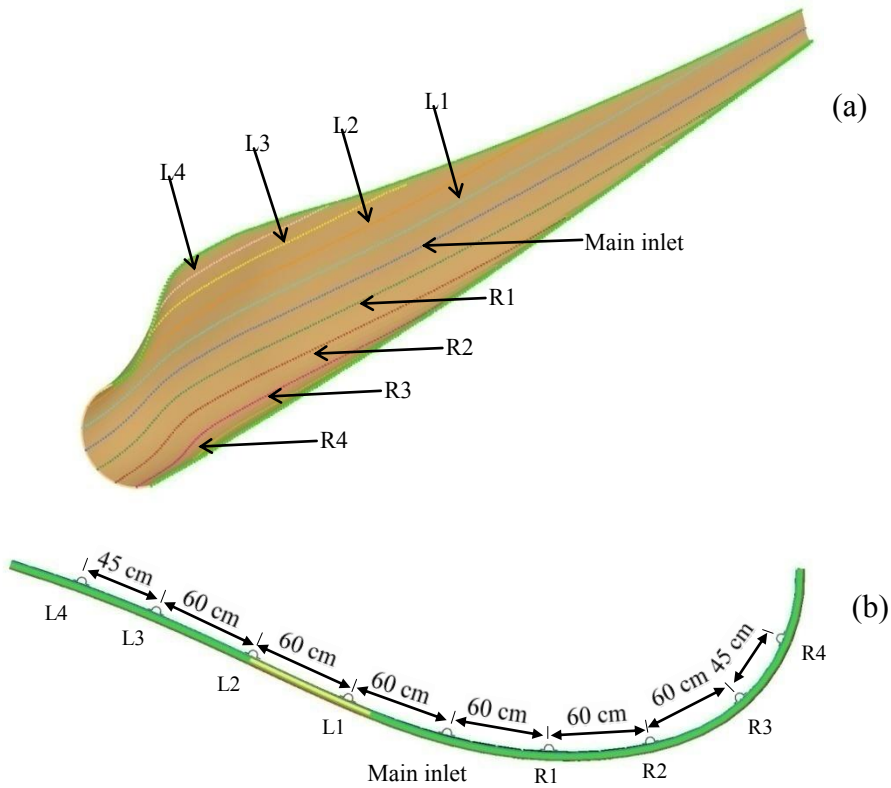

Figure 5.10. (a) Inlet gates and outlet vents positioning for Case 5, (b) Cross section view of the inlet locations.

TABLE 5.4

ACTIVATION TIMES AND FILLING TIMES FOR CASE 5

Inlets	L1	L2	L3	L4	R1	R2	R3	R4	Filling time (Left)	Filling time (Right)
Activation times [s]	1,600	2,600	2,800	3,000	350	700	1,150	1,450	3,756 s	1,990 s

The filling time on the right side of the main inlet is 47% shorter than that of the left side. As it was shown in Table 5.3, using three inlet gates on the right side results in a filling time of 2,571 seconds for that side, which is still less than 3,756 second for the left side, therefore auxiliary gate R4 was considered unnecessary.

5.1.1.6 Case 6: Eleven Inlet Gates

In Case 6, five auxiliary inlets were defined on each side of the main inlet gate with the same distance of 45 cm from each other (see Figure 5.11). The appropriate activation times and the resulting filling times are shown in Table 5.5.

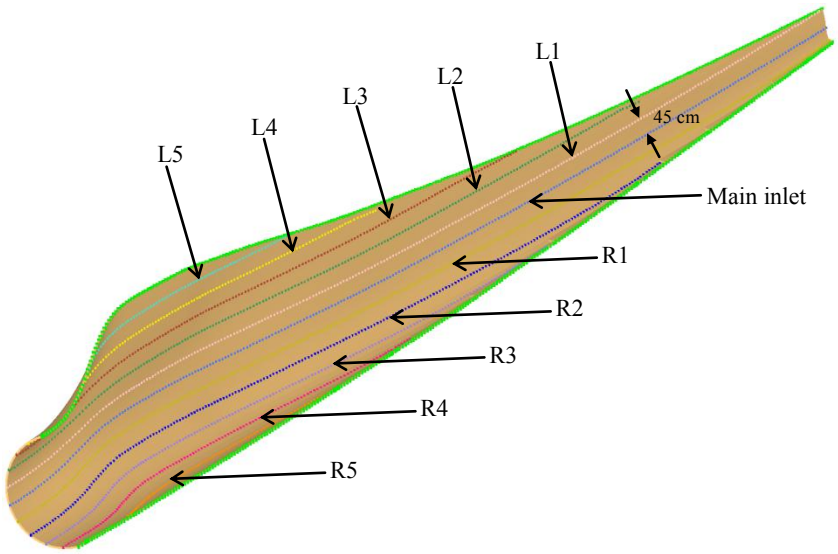

Figure 5.11. Inlet gate and outlet vents positioning for Case 6.

TABLE 5.5

ACTIVATION TIMES AND FILLING TIMES FOR CASE 6

Inlets	L1	L2	L3	L4	L5	R1	R2	R3	R4	R5	Filling time (Left)	Filling time (Right)
Activation times [s]	1,600	2,400	2,700	2,800	2,900	150	350	550	800	1,100	3,671 s	1,642 s

Based on the same explanation made for Cases 4 and 5, Auxiliary gates R4 and R5 can be removed since they have no effect on the overall filling time.

5.1.1.7 Selection of the Optimum Case

Figure 5.12 graphically shows the filling time associated to each case. It shows that as the number of auxiliary gates increases from case to case, the filling time shortens monotonically

and finally goes to a plateau after Case 5; therefore, studying additional cases with more inlet gates was considered unnecessary.

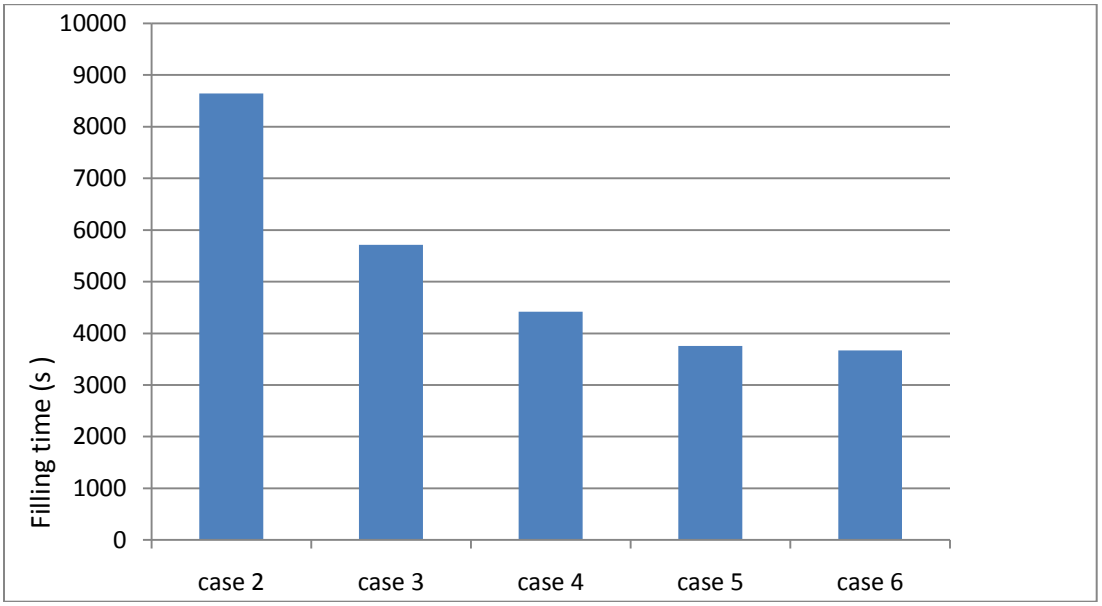

Figure 5.12. Filling times for all studied cases of inlet arrangement.

In order to choose a certain number of auxiliary gates as the optimum case, the effectiveness of the added inlets for each case had to be calculated. In Table 5.6 the first row shows the added length of inlet gate for each case compared to the previous case. In the second row, the resulted shortened filling time from the related previous case is shown. The ratio of shortened time over the added length of inlet gate is shown in the third row. The later value represents the effectiveness of the added inlets in shortening the filling process.

As it can be seen in Table 5.6, the shortened filling time by unit length of added inlet, decreases by half from one case to the next, except for Case 6 in which the value drops dramatically to about 10% of that of Case 5; therefore, the Case 6 was rejected and Case 5 was selected as the optimum case. However, as it was discussed for Case 5, while four auxiliary inlets are used on the left side, using three inlets in the right is sufficient. Therefore, auxiliary

inlet R4 was removed and the inlet arrangement shown in Figure 5.13 was chosen as the optimum arrangement.

It is important to note that a more confident decision on choosing the appropriate number of inlet gates, requires a tradeoff study based on detailed economic information on inlet costs and on profits gained by shortening the filling process.

TABLE 5.6

THE EFFECTIVENESS OF ADDED INLET GATES

	Case 2	Case 3	Case 4	Case 5	Case 6
Added length of inlet compared to previous case (m)	29.7	28.8	24	26.2	30
Filling time Shortened, from the previous case (s)	-------	2,926	1,298	662	85
Filling time shortened by one meter of added inlet	-------	101.6	54.1	25.3	2.83

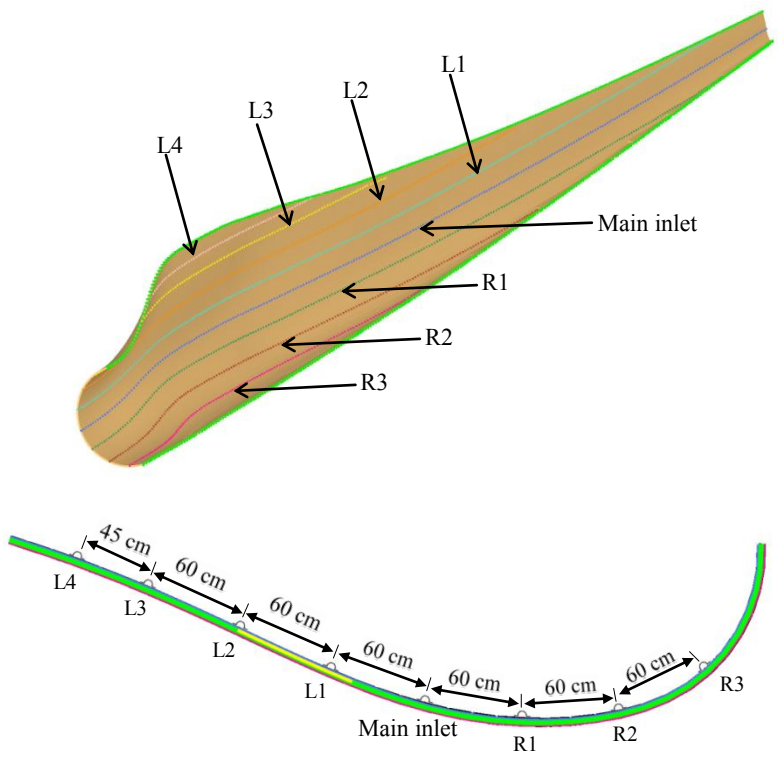

Figure 5.13. The selected arrangement for the inlet gates.

5.1.2 Resin Temperature

After determining the appropriate arrangement for the auxiliary gates, the effect of different resin temperature on shortening the filling process was studied in the second phase of the case study. The inlet arrangement shown in Figure 5.13 was used for all cases of resin temperature. The mold and the preform had the same initial temperature of 330K for all cases.

Since the resin viscosity varies in different temperatures, the arrival time of the flow front to the auxiliary gates changes from case to case; therefore, the inlet activation times were adjusted for each case.

The simulations were conducted for resin temperatures of 300°K, 310°K, 320°K, 325°K, 330°K and 340°K. Different activation times were tried for each case and except for the last case (340°K), a full impregnation of the preform was resulted for all other case. Auxiliary inlet activation times shown in Table 5.7 resulted in the shortest filling times.

TABLE 5.7

ACTIVATION TIMES AND FILLING TIMES FOR THE CASES OF RESIN TEMPERATURE.

Resin Temperature	Auxiliary inlets activation times [s]							Filling time (Left)	Filling time (Right)
	L1	L2	L3	L4	R1	R2	R3		
300 K	1,900	3,000	3,150	3,250	450	850	1,250	4,477 s	3,740 s
310 K	1,700	2,600	2,900	3,000	400	800	1,200	3,939 s	3,124 s
320 K	1,600	2,600	2,800	3,000	350	700	1,150	3,750 s	2,774 s
325 K	1,600	2,600	2,800	3,000	350	700	1,150	3,674 s	2,589 s
330 K	1,700	2,700	3,000	3,000	300	650	1,100	3,712 s	2,349 s
340 K	1,600	2,600	2,800	3,000	280	600	9,50	--------	2,150 s

For the resin temperature of 340°K the flow was not able to fully impregnate the preform and due to high viscosity in some areas the simulation ended incomplete. Figure 5.13 shows the filling pattern, and Figure 5.14 shows the degree of cure at the end of filling, for the mentioned

case. The figure shows that the flow front was clogged in the left side of the main inlet gate leaving a large unfilled area, while on the right side, the preform was fully impregnated.

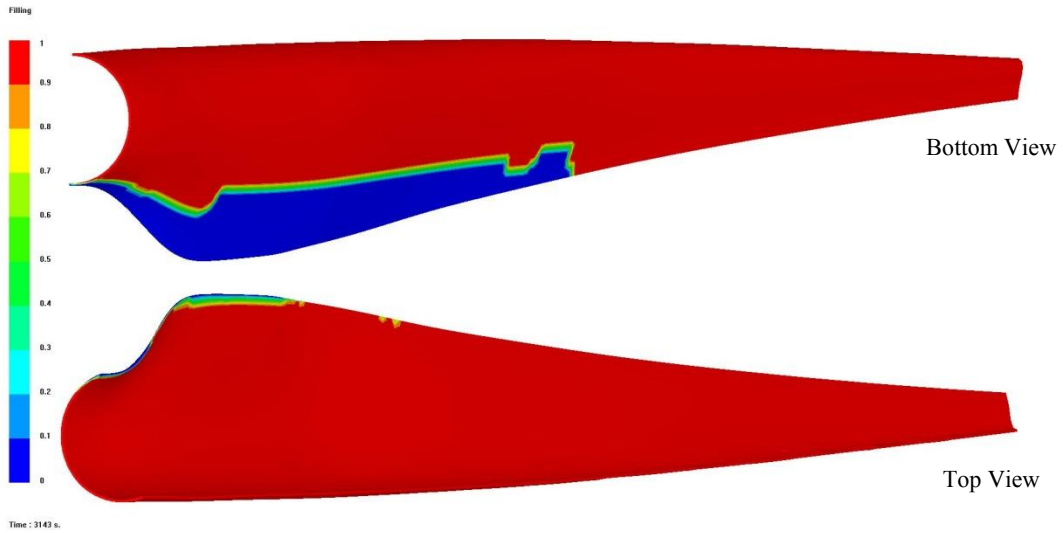

Figure 5.14. Filling pattern for resin temperature of 340°K, at end of filling.

Figure 5.15 for the left side, shows that the resin adjacent to the flow front at the bottom of the part has a high degree of cure (30-55%) which resulted in high viscosity of the resin and blockage of the flow beneath the core. The reason for the significant difference between the degrees of cure on the top and at the bottom of the part is that the resin at the bottom was injected prior to the resin on the top, therefore it had started to cure earlier.

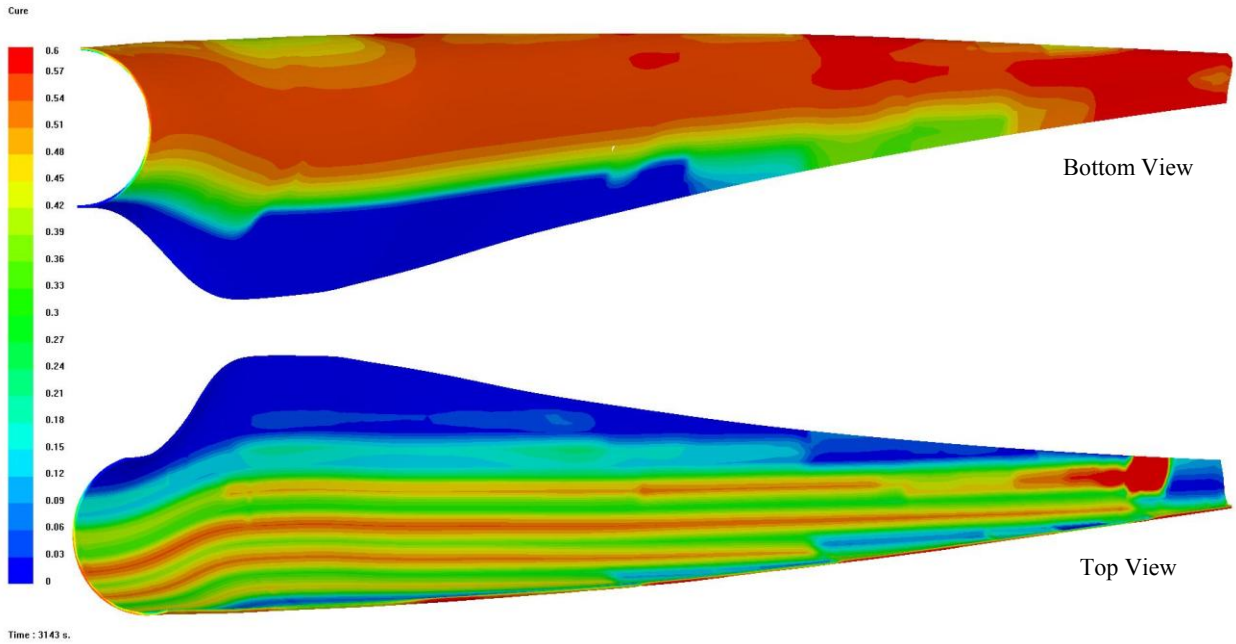

Figure 5.15. Degree of cure for resin temperature of 340°K, at end of filling.

Figure 5.16 graphically shows the filling times associated with each resin temperature for the two sides of the main inlet gate. The resin temperature of 325°K resulted in the shortest filling time and was chosen as the appropriate resin temperature. For higher resin temperatures, the complications associated with the sandwich region, enforced further delay in activations of L1, L2, and L3, which resulted in longer filling times compared to case 325°K.

No delay in activation times was required for the inlet gates located in the right side of the main inlet gate. The resin temperature of 340°K resulted in the shortest filling time in the right side. Increasing the resin temperature from 325°K to 340°K resulted in a decrease of 17% in filling time for that side.

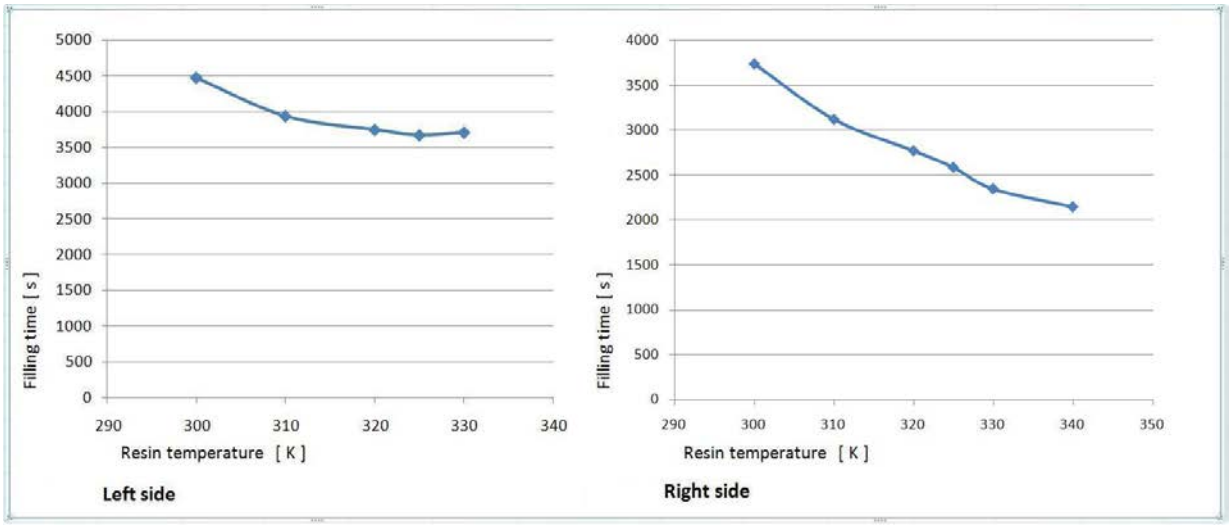

Figure 5.16. Filling times for cases of resin temperature.

5.1.3 Mold Temperature

From the last two phases of case study, the optimum inlet arrangement (shown in Figure 5.13) and the resin temperature (325°K) was selected. In the third phase of the case study, the effect of mold temperature on shortening the filling time was studied. Filling simulations were conducted for mold temperatures of 320°K, 330°K, 335°K, and 340°K. Auxiliary gate activation times shown in Table 5.8 resulted in the shortest filling time for each case.

As it was shown in Table 5.8, changing the mold temperature from its initial value of 330°K did not result in shorter filling times. For the mold temperature of 335°K, a longer delay was required for the activation of auxiliary gate L3 and therefore could not result in a shorter filling time. Mold temperature of 340°K was not able to complete the filling on the left side of the main inlet gate.

TABLE 5.8

ACTIVATION TIMES AND FILLING TIMES FOR THE CASES OF MOLD TEMPERATURE.

Mold Temperature	Auxiliary inlets activation times [s]							Filling time (Left)	Filling time (Right)
	L1	L2	L3	L4	R1	R2	R3		
320°K	1,900	3,000	3,150	3,250	400	800	1,200	4,029 s	2,943 s
330°K	1,600	2,600	2,800	3,000	350	700	1,150	3,674 s	2,589 s
335°K	1,600	2,600	3,000	3,000	300	650	1,100	3,754 s	2,579 s
340°K	1,600	2,600	2,800	3,000	300	650	1,100	--------	2,500 s

5.2 3D Non-isothermal Filling and 3-D Curing Simulations

Compared to the conventional isothermal filling simulations, the non-isothermal filling simulations are considered to be more accurate on estimating the flow pattern. They consider the effects of temperature changes on the flow behavior during filling. This ability is essential for the cases in which temperature variations during the filling process leads to significant changes in resin viscosity. Although non-isothermal filling simulations are accurate, they suffer extensive computation times. For many cases, isothermal flow models can still provide reasonably accurate results, in a timelier manner; cases in which the resin, the mold, and the preform have almost the same temperatures and temperature variations are minimal during filling.

Most simulation models implicated by industry are in 2.5D format where the resin flow is assumed uniform in the thickness. For the cases of relatively thick laminates, 2.5D models are not able to predict flow pattern accurately and therefore, employment of 3-D models has to be considered.

In the following, an analysis on the results of 3-D non-isothermal, 3-D isothermal, and 2.5-D non-isothermal simulations was conducted and by comparing their results, the goal was to evaluate the necessity of using 3-D non-isothermal flow model for this particular part.

5.2.1 Results for 3-D Non-Isothermal Filling Simulation

3-D non-isothermal filling simulation was carried out using the selected process parameters achieved in the case study.

Figure 5.17 shows the filling pattern at different times. As can be seen in the top view, the flow front remained parallel to the main inlet gate in the right side of the main inlet gate, throughout the process. In the left side however, the flow front's velocity increased on the top of the core, and caused the front line to stretch forward in to the sandwich region. Since the high permeability CFM is the only layer on top of the core, the resin tends to flow rapidly in the in-plane direction. Immediately after the sandwich region, the patterns get more compact which shows reduction in flow velocity.

In the bottom view, the compact patterns in the sandwich region show low velocity of the flow beneath the core. Since the core is impenetrable, activation of the auxiliary gates has almost no effect on boosting the flow front beneath the core; therefore, the flow front is relatively slow in that area. The figure shows rapid flow in the last time step (shown as red) near the edge of the wind blade. The activation of auxiliary gates was purposely delayed, to provide enough time for the flow front at the bottom to reach its way out of the sandwich region and converge with the flow from the top. As soon as the lower flow front exited the sandwich region, the remaining auxiliary gates (L2, L3 and L4) were hurriedly activated one after another, therefore, the rest of the part impregnated quickly.

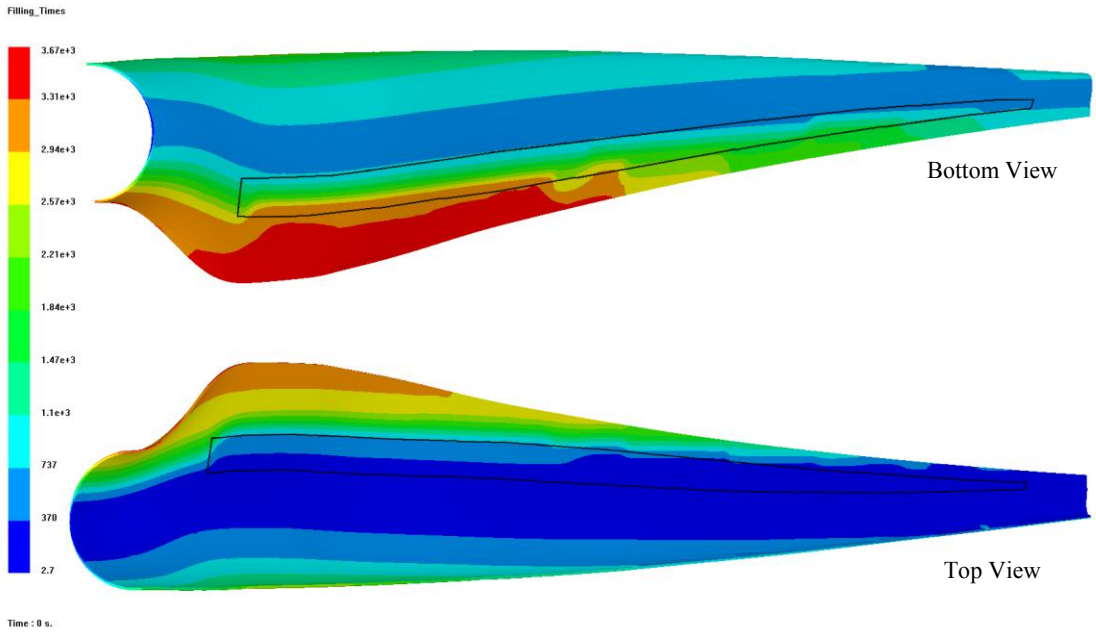

Figure 5.17. Filling pattern of the selected case using 3D non-isothermal filling simulation.

In order to observe the flow pattern in the thickness view, the part was sectioned and the flow pattern for different times was simulated. As it can be seen in 5.18 (a), the flow front in the left side reached a further distance compared to the right side. As it was previously explained, the impenetrability of the core material, and the placement of a high permeability CFM layer on top of the part, accounts for the behavior. The flow front reached both L1 and R1 auxiliary gates at this time (345 s). R1 activates soon afterwards at 350s, conversely the activation of L1 was delayed to 1,600 seconds after filling.

Figure 5.18(b) shows that the flow in the left side had reached the end of the sandwich region through the top layer, and had started to smear downwards. In the right side of the sandwich region, the flow front had already reached the bottom of the part and started to flow in the in-plane direction beneath the core. The in-plane velocity of the flow front was enhanced by assistance of the CFM layer at the bottom.

Figures 5.18 (c) and (d) show the development of the flow front from the top and the bottom of the core material, toward convergence after passing the core.

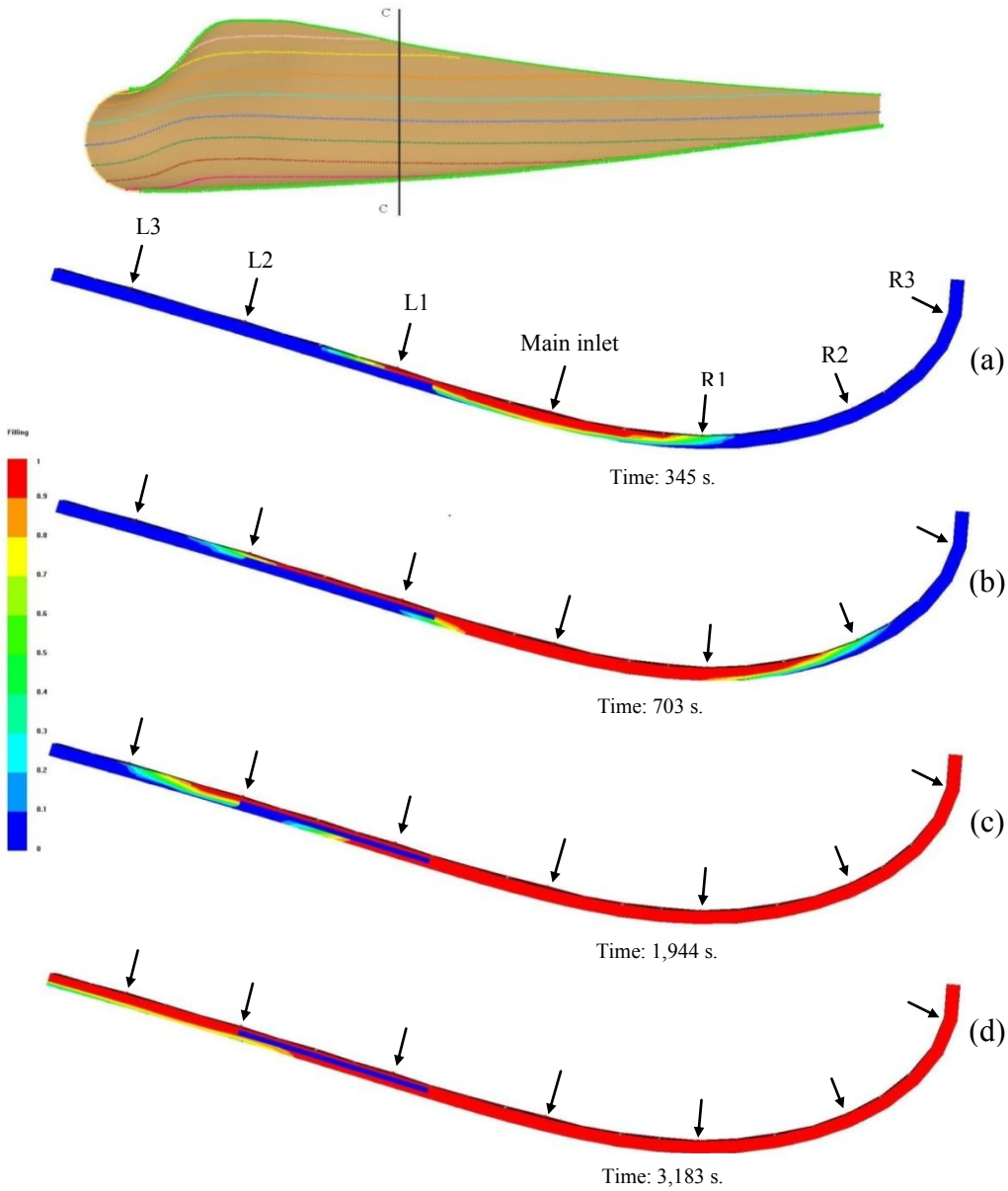

Figure 5.18. Cross section view of filling pattern of the selected case using 3D non-isothermal filling simulation.

5.2.2 Results for 3-D Curing Simulation during Non-Isothermal Filling

The simulation for degree of cure during non-isothermal filling for different times is shown in Figure 5.19. As can be seen in 5.19(a), the first areas to begin curing are the ones adjacent to the edges of the flow front. Since fresh resin is still being injected from the main inlet gate, the resin close to that inlet has zero degree of cure.

Figure 5.19(b) shows that the resin close to the flow front in the left side of the main inlet gate has a relatively higher degree of cure compared to the flow front in the right. The activation of the auxiliary inlets in the right side accounts for the behavior. All auxiliary inlet gates in the right side, had activated at this time (1,433s). The resin close to the flow front was injected from the last activated auxiliary gate (R3) therefore, has a low degree of cure. In the left side of the main inlet gate, on the other hand, none of the auxiliary inlets had activated and all the resin in that side was injected from the main inlet gate. Since this resin was the earliest injected, it reached a higher degree of cure.

Parallel stripes of high degree of cure areas are noticeable in all top views of Figure 5.19. The sequential activation of auxiliary inlet gates accounts for the formation of that pattern. As each auxiliary gate activates, it eliminates the pressure gradient for the previous inlet gate in the upper layers, and compels that inlet gate to reduce its injection level. Therefore, the resin injected from the previous inlet stops flowing further in the upper layers and it stagnates right at the newly activated auxiliary gate. This stagnated resin forms a strip of high degree of cure area, sharply contrasted from the zero degree of cure resin from the newly activated inlet gate.

The front view of Figure 5.19(c) shows a step like curing pattern, close to the edges of the wind blade. Geometry of the part and the arrangement of inlet gates account for the formation of the pattern. Due to the geometry of the part, the length of the auxiliary gates gets

smaller as we move from the center towards the edges of the wind blade. Consequently, a portion of each auxiliary gate can inject resin directly toward the outlet vent, without being obstructed by other auxiliary gates. That portion of the auxiliary gate keeps operating regularly, even after the next auxiliary gates had activated. The continuous injection of fresh resin from that area accounts for the formation of the step-like pattern in the curing simulation.

Figure 5.19(d) shows the degree of cure at the end of filling. In the left side of the main inlet gate, a significant difference between the degrees of cure in the area after the core, and the rest of the part is noticeable. The resin from L3 and L4 auxiliary inlet gates impregnated the preform in the area after the core. Those auxiliary gates were the last to activate, therefore, the resin injected from them has the lowest degree of cure. It is important to note that when the resin on top of the part passes the core, it flows downward and converges to the lower flow front. This stops the resin at the bottom from flowing further. Since the resin at the bottom of the core was injected much earlier, it has a significantly higher degree of cure, compared to the resin after the location of convergence.

Figures 5.19(c) and 5.19(d) show higher degree of cure for the sandwich region compared to other areas. This mainly takes place due to the heat transfer from the initially 5°K warmer core material. Due to the existence of an impenetrable core, the overall amount of resin is comparatively low in that area and therefore the temperature rises relatively fast and accelerates the curing. It is also important to consider that the resin beneath the core was injected from the main inlet gate, which was the first inlet gate to activate. The resin was stagnated right at end of the core and was not blended with the fresh resin from the auxiliary gates. Because this resin was injected earlier than the resin in other areas, it reached a higher degree of cure.

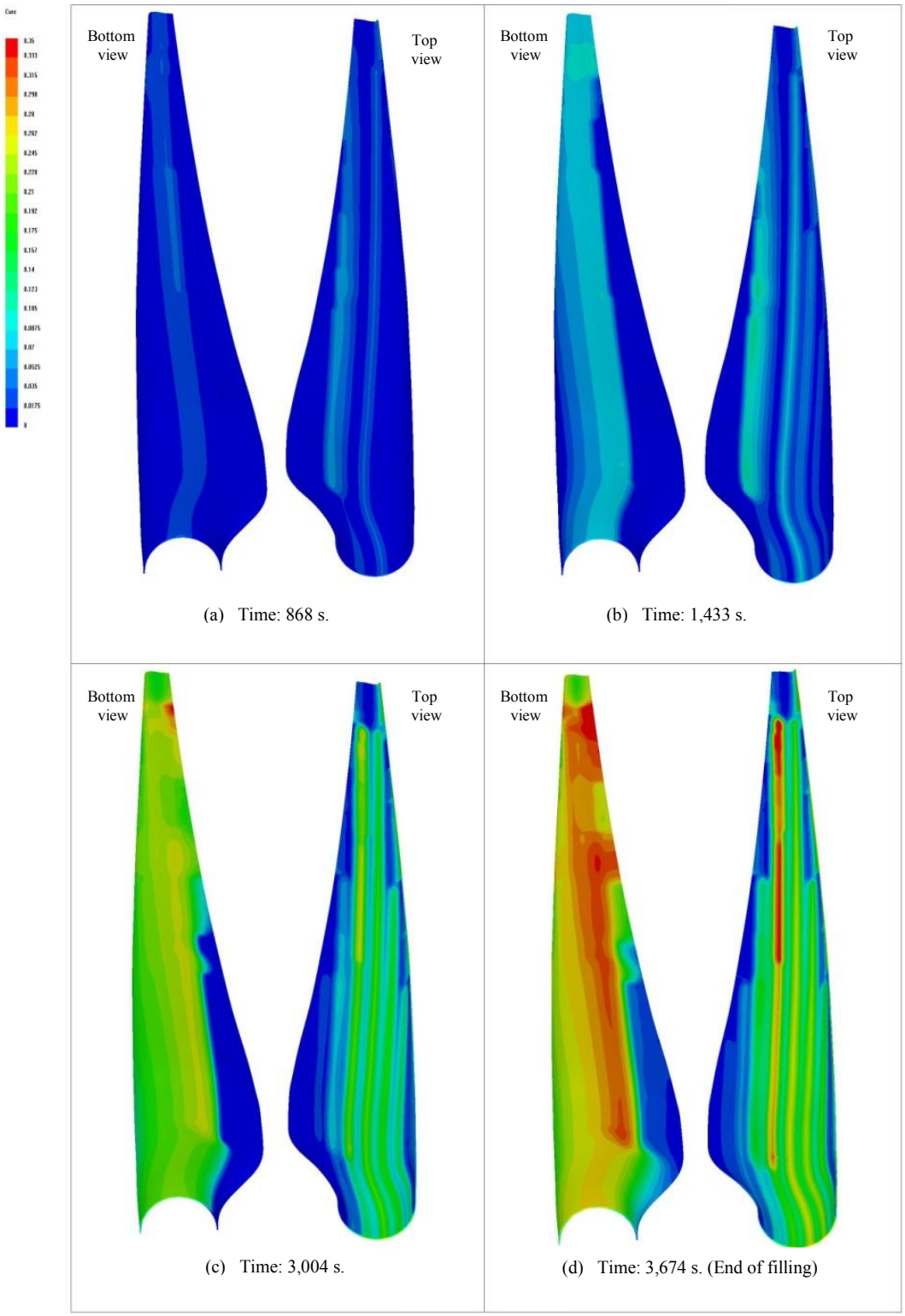

Figure 5.19. Degree of cure during 3D non-isothermal filling.

5.2.3 Results for 3D Curing Simulation after Non-Isothermal Filling

The curing and thermal state of the part at the end of filling was imported into the curing model to simulate the cure after the end of filling; the results for degree of cure are shown in Figure 5.20.

Figure 5.20(b) shows a higher overall degree of cure for the left side of the main inlet gate, compared for the right side. The reason lies in the occurrence of resin bleeding from the right side outlet vent during the filling process. Filling stage for the right side was completed in 2,589 seconds, whereas for the left side it took 1,085 seconds more. In the period after the completion of filling in the right side, the auxiliary gates in that side were still active, so the injection of the fresh resin caused the earlier injected resin to escape from the right side outlet vent. For the left side on the other hand, resin bleeding was minimal and limited to areas close to the tip. Therefore the earlier injected resin remained inside the part, and made the left side's curing to be ahead of the right.

An important observation in the figure is that even though the resin in the sandwich region had the highest degree of cure at the end of filling, but as the time progressed, the surrounding areas cured in a faster pace and reached higher degrees of cure. To give an explanation, it has to be considered that the generated heat from the curing reaction tends to increase the reaction rate. More resin means more heat, and more heat causes a faster curing process. Since there is no resin inside the core material, less heat was generated in sandwich region, and in the end, the degree of cure in the resin-rich surrounding areas exceeded.

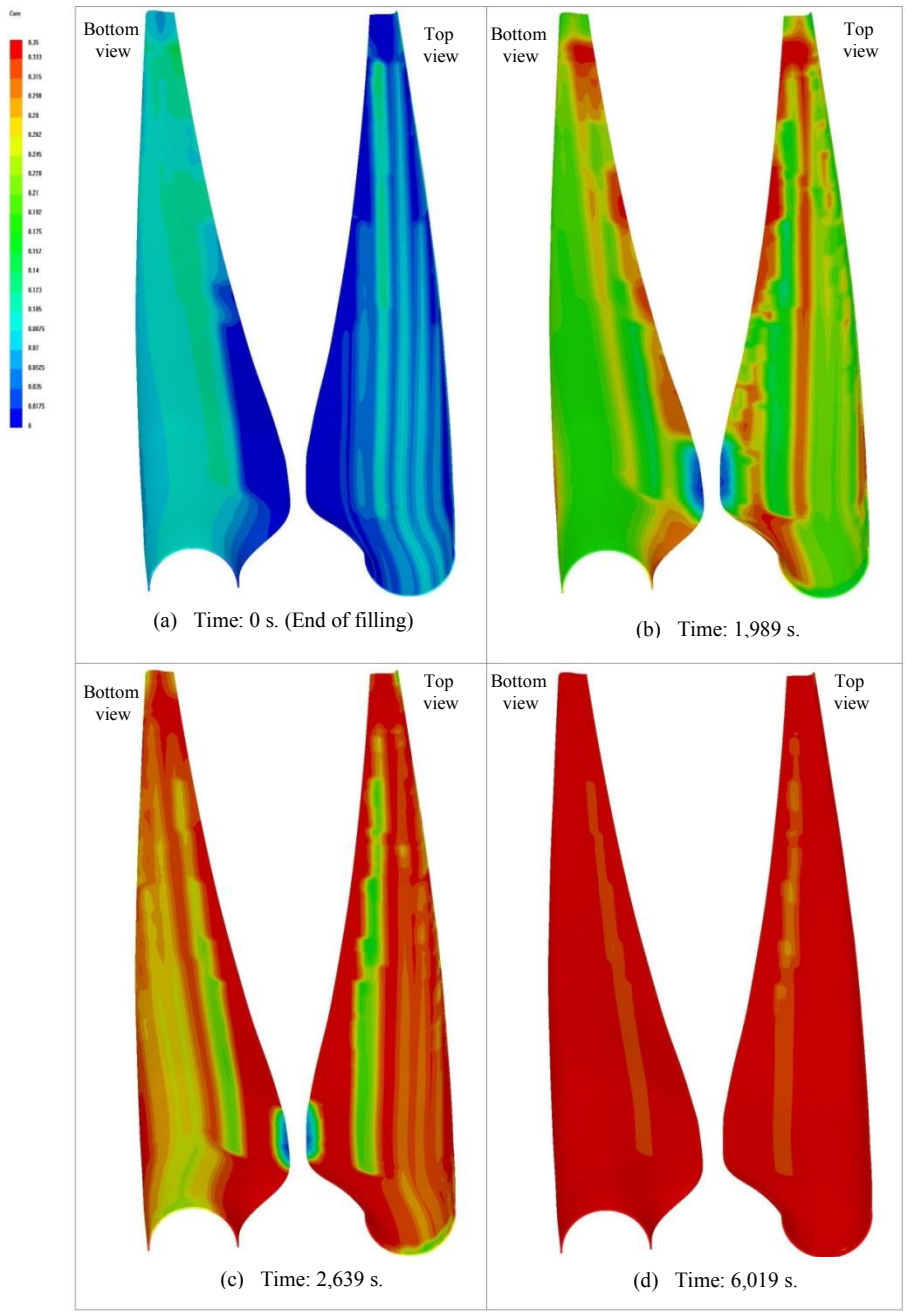

Figure 5.20. Degree of cure after non-isothermal filling.

In aid to have a better comparison between the curing behaviors of the sandwich region and the main region, Figure 5.21 graphically shows the curing history of those areas. The location of the cross section in which the measuring points are located is the same as it was in Figure 5.18. Points A and B are located on the top and at the bottom of the core material, and

represent the sandwich region. Point C is located on top of the part, away from the core, and represents the main region.

The Figure shows significant difference between the curing behaviors of sandwich and main regions. Resin at point C had a lower degree of cure at the end of filling, but as the time progressed the curing rate accelerated, resulting its degree of cure to exceed the ones of A and B at around 1,600 seconds after the end of filling.

The Figure shows that the resin in the sandwich region was not able to reach full degree of cure and was eventually limited to 96% after 13,000 seconds. For the sandwich region, the figure shows that the curing at point B was faster compared to the curing at point A; however, the final cure state was the same for both points at the end of the cycle. This is basically because there is an additional layer of biaxial at the bottom of the core. The additional layer means additional resin that due to its curing, generates heat and increases the reaction rate.

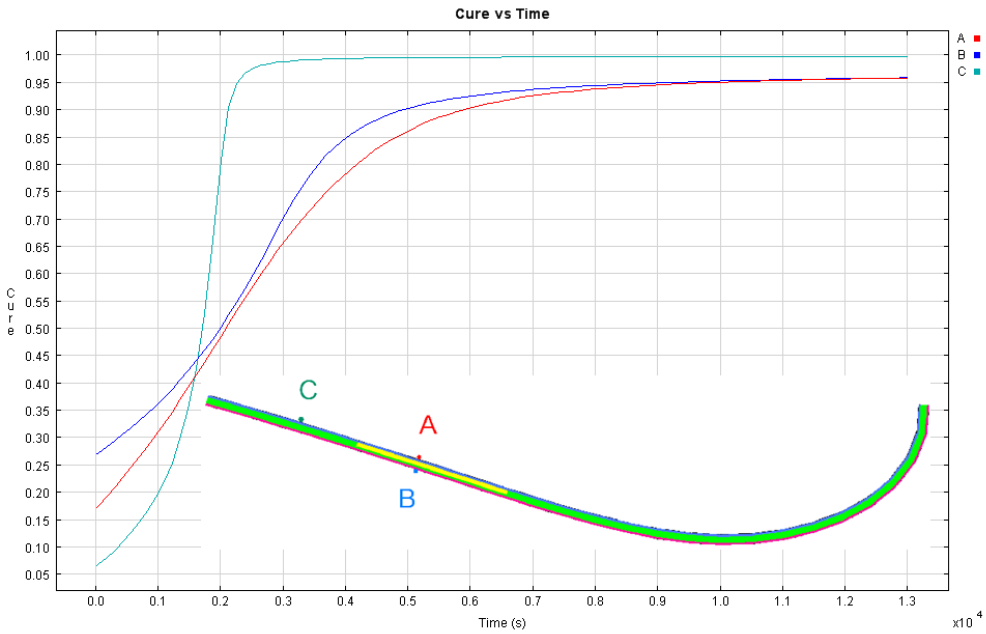

Figure 5.21. Curing history of the indicated points, after end of filling.

5.2.4 Results for Temperature Distribution while Curing after Non-Isothermal Filling

Figure 5.22 shows the temperature distribution while curing at different times. As it can be seen in Figure 5.21(a), the sandwich region was the warmest area at the end of filling; this, however, changed quickly and the temperature of the neighboring areas (shown in color red in 4.22b) exceeded. The temperature in those areas started to increase rapidly at around 600s and eventually reached the highest temperature of 420°K at around 2,250s. The temperature in the sandwich region increased at a much slower rate compared to the neighboring areas and reached the maximum of 372°K at around 3,200s.

Figures 5.22(c) and 5.22(d) show a gradual decrease in temperature, which is a result of releasing the heat via convection with the ambient air. Figure 5.22(d) shows that in 13,000 seconds after the end of filling, the areas closer to the edges have cooled down to the ambient temperature while the areas in the middle of the part are warmer. This is basically due to the difference between the heat transfer coefficients of the two areas.

Figure 5.23 shows the temperature history of the same three points shown in Figure 5.21. As it can be seen in the figure, the temperature of point B reached the highest temperature of 370°K at around 3,200s while point A reached the highest temperature of 364°K at 5,200s. This explains the faster curing of point B and also demonstrates the mutual relation between temperature and reaction rate.

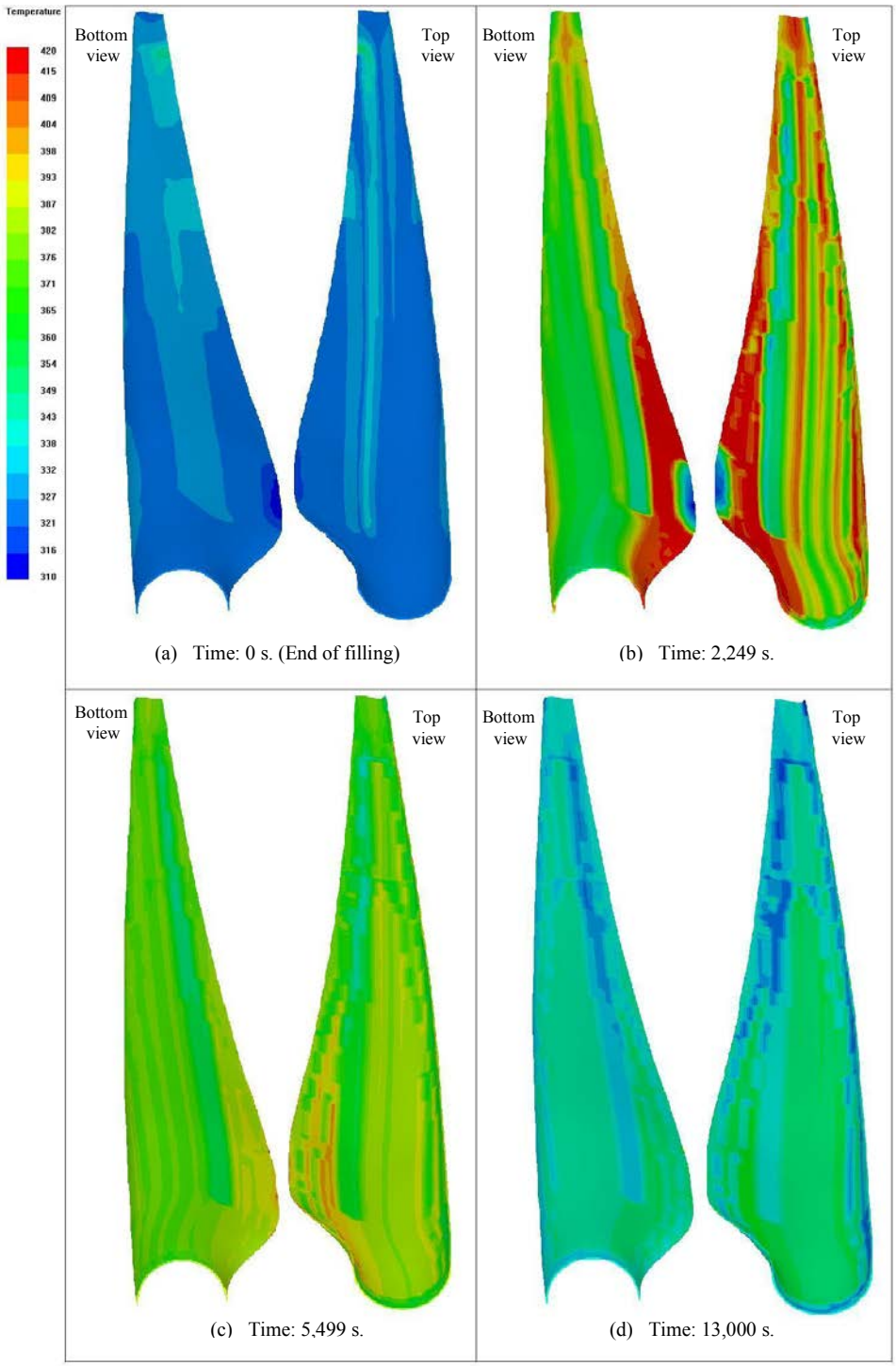

Figure 5.22. Temperature distribution during cure, after non-isothermal filling.

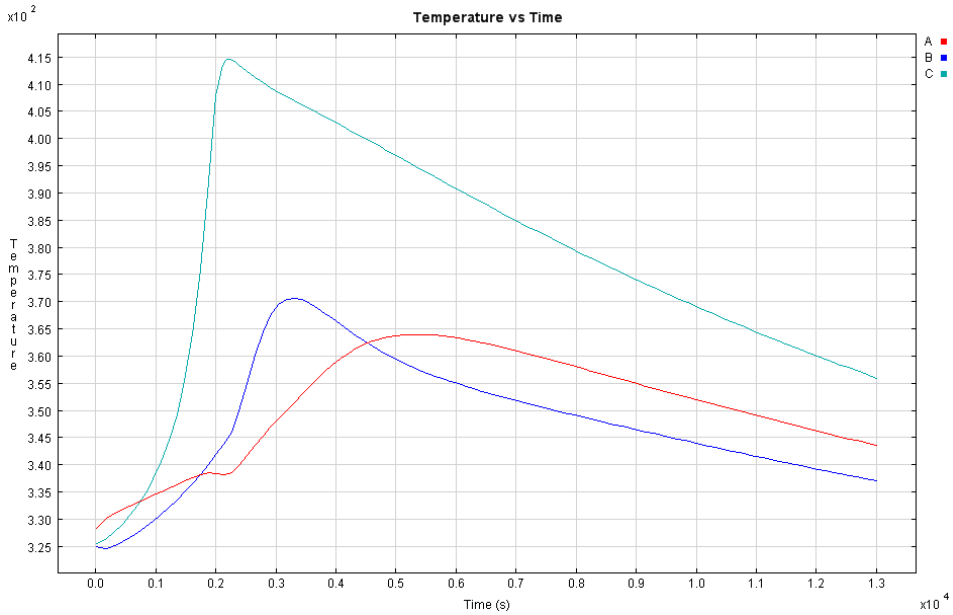

Figure 5.23. Temperature history of the points indicated in Figure 5.21.

5.3 2.5-D Non-Isothermal Filling Simulation and Comparison with the 3-D Non-Isothermal Simulation

The same process parameters that were used for the 3D non-isothermal simulation, were used for the 2.5D non-isothermal simulation. Results for the filling pattern are shown in Figure 5.25.

The figure shows that the flow front remained parallel to the main inlet gate throughout the process and no significant difference in flow behavior was observed between the sandwich region and main region. This particularly demonstrates the shortcoming of the 2.5D model on predicting the velocity changes around the core material.

The results show filling times of 1,841s for the right side and 3,182s for the left side of the main inlet gate. These filling times are significantly shorter than the filling times obtained by the 3-D non-isothermal model. In the 3D simulation, the resulted filling times were 2,589s for

the right side and 3,674s for the left, which, compared to the 2.5D model, shows a decrease of 30% and 13%, respectively.

The reason for the large difference in filling times lies in the fundamental differences between the two models. In the 3-D model the inlets were defined on the top of the part, while for the 2.5-D model doing the same is not possible and any condition that is defined for an element will be considered for the whole thickness. In a 2.5-D model when a row of elements is defined as an inlet gate, it is assumed that the injection takes place uniformly for the whole thickness.

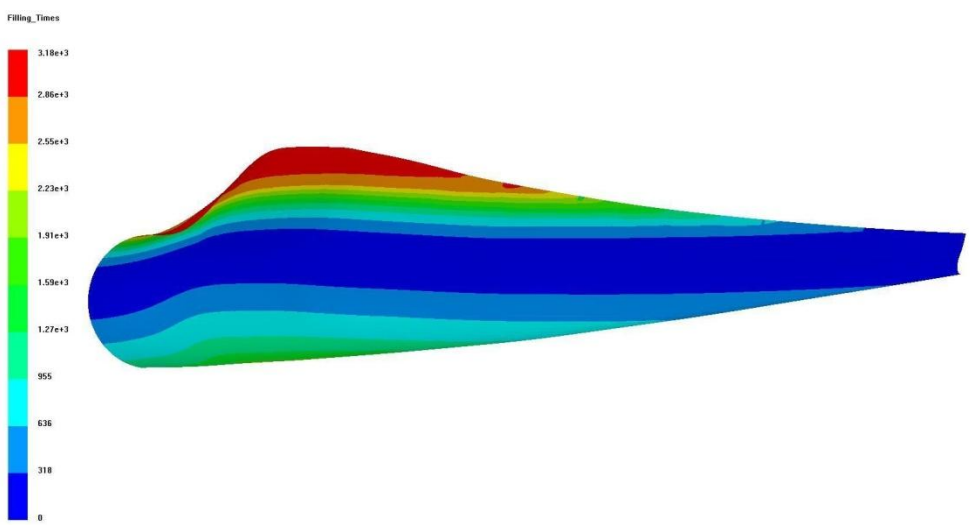

Figure 5.24. Filling pattern from 2.5-D non-isothermal filling simulation.

To investigate, and verify the aforementioned reason for the difference in filling times, a modified version of the 3-D non-isothermal filling simulation was conducted. The inlet gates were defined with the same arrangement but instead of defining them only for the top layer, they were extended through the thickness so the resin could be injected in all layers at the same time. Although impractical in reality, the later simulation was essential to assure that the difference in results was not caused by a software deficiency or personal error. The resulted filling pattern is

shown in Figure 5.25. The results show filling times of 1,970s for the right side and 3,196s for the left, which in comparison to the 2.5-D results are very close. In addition, the similarity between the filling patterns shown in Figures 5.23 and 5.24 proves the aforementioned reasons. Since the resin is injected from all layers, minor differences can be observed between the top and bottom views of Figure 5.24.

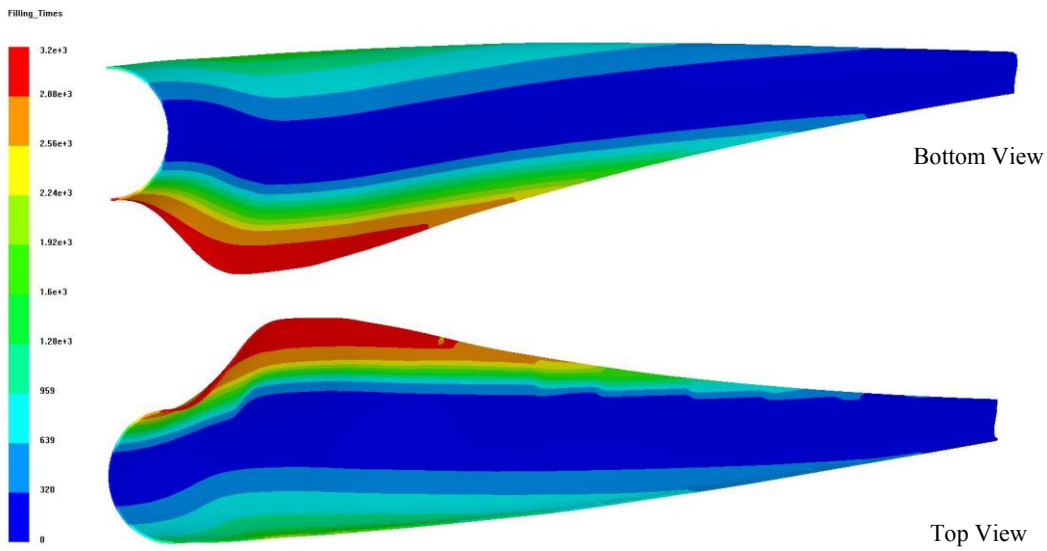

Figure 5.25. Filling pattern from the altered version of 3-D non-isothermal filling simulation.

It is important to note, that the process parameters applied for the 2.5-D non-isothermal model were obtained by the 3-D non-isothermal model. A more accurate approach to comparing the results of 3-D and 2.5-D filling simulations is to obtain the selected parameters independently using the two models and, then, compare the results. Doing so was considered unnecessary at this point because even though the same process parameters were used for the two simulations, the differences in the results are already unacceptably high. Since the 2.5-D model was unable to consider the complications in the sandwich region, obtaining the parameters independently by the 2.5-D model would obviously increase the difference between the results.

5.4 3-D Isothermal Filling Simulation and Comparison with the 3-D Non-Isothermal Simulation

Unlike for non-isothermal filling simulations in which resin's viscosity is calculated by the model in every time step, isothermal simulations use a constant value for viscosity throughout the process. The viscosity can either be measured using a viscosity meter or can be obtained from the viscosity model of the resin. In the recent case, degree of cure of the resin was assumed to be zero and the temperature was assumed to be 325°K. These values were substituted into the viscosity model (Equation 4.9) and the viscosity value of 0.19 Pa.s was obtained. The same Inlet arrangement and activation times used for non-isothermal filling simulation were applied for the 3-D isothermal model.

The results of filling simulation at various times are shown in Figure 5.24. Filling process was completed at 2,985s for the right side and 3,820 seconds for the left. Comparing to the 3-D non-isothermal simulation, the increase in filling times was 15% for the right side and 4% for the left. Apart from filling times, no significant difference in flow behavior with 3-D non-isothermal case was observed.

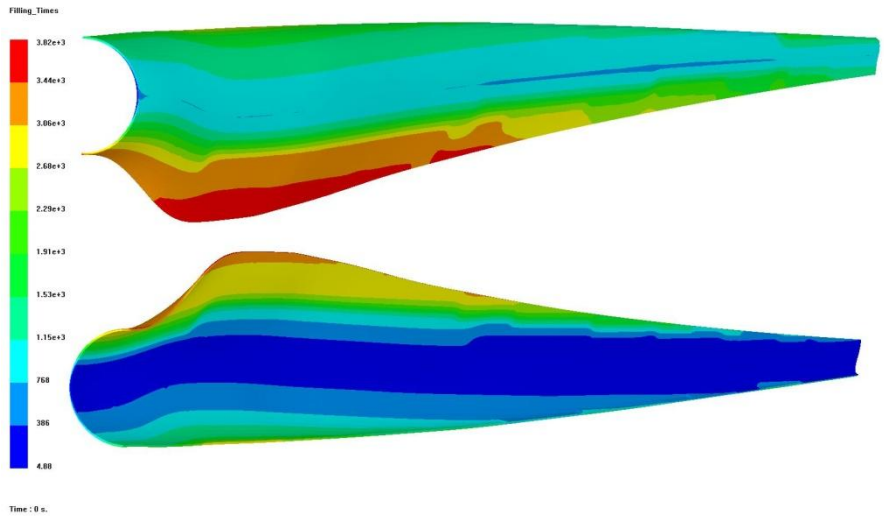

Figure 5.26. Filling pattern from 3-D isothermal filling simulation.

CHAPTER 6

CONCLUSIONS

6.1 Conclusions

3-D flow pattern and cure modeling tools are highly desired by engineers in the manufacturing of new wind turbine blades. In the current work, a 3-D non-isothermal flow model for a wind turbine blade was developed. The model takes into account the resin flow, heat transfer, and cure kinetics. The model is able to track filling pattern, degree of cure, temperature distribution, pressure distribution, and resin loss.

The computer model was utilized in a case study to investigate the effects of inlet arrangement, resin temperature, and mold temperature on filling time. Sequential scheme was selected as the filling strategy. In the first phase of the case study, different inlet arrangements and activation times were used to achieve the shortest filling time. It was observed that as the number of inlet gates increased, its effect on shortening the filling time kept decreasing monotonically. For all the cases, complicated flow behavior was observed in the sandwich region, resulting in large dry spots beneath the core. To overcome the problem, delayed activation times were applied to the auxiliary gates located in the left side of the main inlet gate. At the end of phase one, a modified version with a total number of 8 parallel inlet gates was selected as the best case. This arrangement was then used for all cases of the other phases of the study.

In the second phase of the study, filling simulations for different resin temperatures were conducted. Resin temperature of 325°K resulted in the shortest filling time. Higher resin temperatures required longer delays for activation of the auxiliary inlet agates located in the left

side of the main inlet, therefore, resulting in longer filling times. For the right side of the main inlet gate, on the other hand, increasing the resin temperature from 325°K to 340°K decreased the filling time by 17%.

The effect of different mold temperatures on filling time was examined in the third phase of the study. Increasing the mold temperature above the initial value (330°K) did not result in shorter filling times. It should be considered that in the second phase of the study, the resin temperature was increased to its limit, where further increase in the temperature resulted in longer or incomplete filling. Therefore, higher mold temperatures cause an increase in resin temperature, which consequently leads to the same problem.

Curing results from the best case show that the degree of cure in the sandwich region did not reach higher than 96% during 6 hours after the end of filling. In addition, the results for temperature distribution for that area show an average of 45°C lower temperature compared to other areas. This demonstrates the need for applying external heat to that area for achieving a full cure.

To investigate the necessity of employing 3-D non-isothermal model, a 2.5-D non-isothermal model and a 3-D isothermal model were developed. The selected process parameters, achieved in the case study were applied to both new models and the results were compared to the results from the 3-D non-isothermal model.

The 2.5-D non-isothermal model was unable to show the flow issues in the sandwich region. In addition, although the same inlet arrangement and activation times were used for both 2.5-D non-isothermal and 3-D non-isothermal models, the predicted filling times for the 2.5-D model were 13% and 30% shorter for the left side and right side of the main inlet gate, respectively. The difference in filling times would obviously worsen if the inlet arrangements

and filling times were to be obtained independently using the 2.5-D model. The aforementioned issues support the fact that the 2.5-D simulations are not accurate in predicting the flow pattern in thick parts.

For the 3-D isothermal model, the predicted flow pattern was very similar to that of the 3-D non-isothermal model and the difference in filling times was relatively small. However, since the isothermal model does not involve temperature variation and curing during filling, the simulation of cure after filling would not provide accurate results.

6.2 Recommendations for Future Work

The problem with the slow moving flow front at the bottom of the core, imposed delays the activation of the auxiliary inlet gates. Adding a high permeability layer or creating flow channels (slots) at the bottom of the core may ease the resin flow beneath the core and, therefore, allow earlier activation times. This may significantly reduce the overall filling time and, thus, an investigation of the effects of such techniques on the filling process is recommended.

Sequential filling was chosen as the filling scenario for the case study. Separate studies using other scenarios such as fishbone scheme are recommended.

In this study, different inlet arrangements, activation times, resin temperatures, and mold temperatures were tried to reduce the filling time. A more complete study may involve other issues such as resin loss, thickness variation, void content and fiber volume fraction of the part.

REFERENCES

REFERENCES

[1] Butyon, T., D. Sharpe, N. Jenkins, and E. Bossanyi. Wind Energy Handbook. WILEY, 2001.

[2] Pfund, B. "Resin infusion in the US marine industry." Reinforced Plastics 38, no. 12 (1994): 32-34.

[3] Griffin, D. A. "Blade System Design Studies Volume I: I Composite Technologies for Large Wind." SAND REPORT (Sandia National Labratories) SAND2002-1879 (July 2002).

[4] Goren, A., and C. Atas. "Manufacturing of polymer matrix composites using vacuum assisted resin infusion molding." Archives of Materials Science and Engineering 34, no. 2 (2008): 117-120.

[5] Sayre, J. R. "Vacuum-Assisted Resin Transfer Molding (VARTM) Model Development, Verification, and Process Analysis." Phd Dissertation. Virginia Polytechnic Institute. April 2000.

[6] Markicevic, B., D. Heider, S. G. Advani, and S. Walsh. "Stochastic modeling of preform heterogeneity to address dry spots formation in the VARTM Process." Composites Part A: Applied Science and Manufacturing, 2005: 851-858.

[7] Yoon, M., J. Baidoo , and J. W. Gillespie, Jr. "Vacuum Assisted Resin Transfer Molding (VARTM) Process Incorporating Gravitational Effects: A Closed-form Solution." Journal of Composite Materials, 2005: 2227-2242.

[8] Simacek, P., and S. G. Advani. "Modeling resin flow and fiber tow saturation induced by distribution media collapse in VARTM." Composites Science and Technology, 2007: 2757-2769.

[9] Bayldon, J. M., and I. M. Daniel. "Flow modeling of the VARTM process including progressive saturation effects." Composites Part A: Applied Science and Manufacturing, 2009: 1044-1052.

[10] Koefoed, M. S. "Modeling and Simulation of the VARTM Process for Wind." PhD Dissertation. Aalborg University, 2003.

[11] Mazumdar, S. K. Composite Manufacturing :material, product, . CRC Press, 2002.

[12] Swanson, S. R. Advanced Composite Materials : Introduction to Design and Ana- lysis. Prentice Hall, 1997.

[13] Bishop, W. High Performance Fibers in advanced composites. Elsevier, 1989.

[14] Brøndsted, P., H. Lilholt, and A. Lystrup. "COMPOSITE MATERIALS FORWIND POWERTURBINE BLADES." (Annual Review of Materials Research) 35 (2005).

[15] Griffin, D. A., and D. A. Roberts. "Alternative Materials for Megawatt-Scale Wind Turbine Blades." A collection of technical papers; 44th AIAA Aerospace sciences meeting 19 (january 2006): 14536-14552.

[16] Veers, P. S., T. D. Ashwill, and D. A. Griffin. "Trends in design, Manufacture and Evaluation of Wind Turbine Blades." Wind energy 6, no. 3 (July/September 2003): 245-259.

[17] Cheng-Huat, O., and S. W. Tsai. "The Use of Carbon Fibers in Wind Turbine Blade Design:A Seri-8 Blade Example." SAND2000-0478 (Sandia National Laboratories), 2000.

[18] Penczek, P., P. Czub, and J. Pielichowski. "Unsaturated polyester resins; Chemistry and technology." Advances in polymer science (Springer), 2005.

[19] May, C. A. Epoxy Resines; Chamistry and Technology. Marcel Dekker, 1988.

[20] Thomsen, O. T. "Sandwich Materials for Wind Turbine Blades – Present and Future." Journal of Sandwich Structures and Materials 11 (2009).

[21] Berggreen, C., K. Branner, J. F. Jensen, and J. P. Schultz. "Application and Analysis of Sandwich Elements in the Primary Structure of Large Wind Turbine Blades." Journal of Sandwich Structures and Materials 9 (2007).

[22] http://www.tpicomposites.com/?id=9 (accessed March 9, 2010).

[23] Locke, J., and U. Valencia. "Design Studies for Twist-Coupled Wind Turbine Blades." SAND2004-0522 Unlimited Release June 2004, 2004.

[24] Advani, S. G. Process modeling in composites manufacturing . Marcel Dekker, 2003.

[25] PAM-RTM. ESI Group. 2008. http://www.esi-group.com/corporate/news-media/press-releases/2008-english-pr/esi-group-announces-release-of-pam-rtm-2008.

[26] Darcy, H. P. "Les fontainspubliquesde la villede Dijon." 1856.

[27] Hofmann, J. R., and P. A. Hofmann. "Darcy's Law and Structural Explanation in Hydrology." Proceeding of the 1992 Biennial Meting of the Philosophy of Science Association 1 (1992): 23-35.

[28] Amyx, J. W., D. M. Bass and R. L. Whiting. Petroleum Reservoir Engineering: Physical Properties. 1960.

[29] Calado Veroˆnica, M. A., and S. G. Advani. "Effective average permeability of multi-layer preforms in resin transfer molding." Composites Science and Technology 56, no. 5 (1996): 519-531.

[30] Diallo, M. L., R. Gauvin, and F. Trochu. "Experimental analysis and simulation of flow through multi-layer fiber reinforcment in liquid composite molding." Polymer Composites 19 (1998): 246-256.

[31] Lundstrom, T. S., B. R. Gebart, and E. Sandlund. "In-Plane Permeability Measurements on Fiber Reinforcements by the Multi-Cavity Parallel Flow Technique." Polymer Composites 20, no. 1 (1999).

[32] Gebart, B. R., and P. Lidstrom. "Measurement of In-Plane Permeability of Anisotropic Fiber Reinforcements." 17, no. 1 (FEBRUARY 1996): 43-51.

[33] Lai, Y., B. Khomami, and J. L. KardoS. "Accurate Permeability Characterization of Preforms Used in Polymer Matrix Composite Fabrication Processes." Polymer Composites 18, no. 3 (June 1997).

[34] Kamal, M. R., and S. Sourour. "Kinetics and thermal characterization of thermoset cure." Polym.Eng.Sci., 1973: 59-64.

[35] Theriault, R.P., T.A. Osswald, and J.M. Castro. "Numerical Model of the Viscosity of an Epoxy Prepreg Resin System." Polymer Composites, 1999: 628-633.

[36] Hubert, P., A. Johnston, A. Poursartip, and K. Nelson. "Cure kinetics and viscosity models for Hexcel 8552 epoxy resin ." Soc. for the Advancement of Material and process engineering, 2001: 2341-2354.

[37] Kiuna, N., C. J. Lawrence, Q. P. V. Fontana, P. D. Lee, T. Selerland, and P. D. M. Spelt. "A model for resin viscosity during cure in the resin transfer moulding process ." Composites Part A: Applied Science and Manufacturing, 2002: 1497-1503.

[38] Henne, M., C. Breyer, and M. Niedermeier. "A New Kinetic and Visco- sity Model for Liquid Composite Molding Simulations in an Industrial Environment." Polymer Composites, 2004: 255-269.

[39] Ngo, N. D., R. V. Mohan, P. W. Chung, K. K. Tamma, and D. R. Shires. "Recent Developments Encompassing Non-Isothermal/Isothermal Liquid Composite Molding Process Modeling/Analysis: Physically Accurate, Computationally Effective, and Affordable Simulations and Validations." Journal of Thermoplastic Composite Materials, 1998: 493-532.

[40] Berry, D. Wind Turbine BladesManufacturing Improvements and Issues. TPI Composites, Inc. February 24, 2004. http://www.sandia.gov/wind/2004BladeWorkshop-PDFs/DerekBerry.pdf.

[41] Chan, A. W., and R. J. Morgan. "Sequential multiple port injection for resin transfer molding of polymer composites." S.A.M.P.E. Quarterly 24 (October 1992): 45-49.

[42] Nolet, S. C. Wind Turbine blades: Building Reliability. TPI Composites, Inc. june 18, 2009. http://www.sandia.gov/wind/2009Reliability/PDFs/Day2-09-StephenNolet.pdf.

[43] Bauccio, M. ASM International. ASM Engineered Materials Reference Book. Second Edition. Materials Park, OH, 1994.

[44] Lee, S. S., and S. C. Kim. "Analysis of unsaturated polyester-polyurethane interpenetrating polymer networks.I: reaction kinetics and viscosity model." Polymer Engineering and Science, 1991: 1182-1188.

[45] Lee, D. S., and C. D. Han. Polymer Engineering & Science, 1987 : 955.